Chapter- 3

Results and Discussion

3. Results and Discussion

This chapter has been subdivided into 5 different sections as mentioned below-

1. Hammer milling of WPCBs and optimization of parameter
2. Delamination of WPCBs by dissolution of HER in DMF
3. Liberation of WPCB's metal-clad by HER dissolution using DMA
4. Comparative study of HER dissolution in DMA *vs.* DMF and study of mechanism
5. Delamination of large size WPCBs and post-treatment leaching of copper

Section- 1

Hammer milling of WPCBs and optimization of parameters

3.1 Hammer milling of WPCBs and optimization of parameters

The chopped WPCBs of 2.25 cm^2 size has been crushed to –1 mm size by using hammer mill under varying feed rates and time and the results have been discussed. The WPCBs has been crushed to -1 mm as it results in maximum liberation of metal and nonmetal fractions [83].

3.1.1 Effect of time on milling of WPCBs

To study the effect of time on the milling of WPCBs to –1 mm, the preliminary experiments were carried out at feed rate 3 $kg \cdot h^{-1}$. **Figure 3.1** shows the variation of undersize (–1 mm) and oversize (+1 mm) fraction after different milling time. It is evident that the undersize fraction increases with increase in the milling time. **Figure 3.1** also elucidates that 37 % of fed WPCBs is ground to –1 mm in 30 sec. Nature of curve shows higher slope values (m) up to 1.5 min (m= 47.9) that indicates relatively faster milling during that period. This is because the impact forces transferred by the swinging hammers result in the quick fracture of the rigid structure of WPCBs. Data also shows that after 1.5 min nearly 72 % of fed WPCBs are crushed to –1 mm. The chemical analysis of milled WPCBs after 1.5 min showed the presence of a majority of non-metallic fraction along with 5.8 wt% copper (**Table 3.1**). This is because the non-metallic fraction of WPCB (glass fibre and cured resin) is brittle in nature and can be crushed rapidly. Later, the slope of the curve is decreased (m= 4.03) because the ductile metal fraction of WPCBs gets elongated initially and then only its size reduction takes place. The chemical analysis of milled WPCBs after 7 min also elucidates the presence of ~22 wt% copper. After 7 min, 94 % of fed WPCB were crushed to –1 mm and the slope of curve tends to be flattened at a value of 0.123 as shown in **Figure 3.1**. Based on

the above observation it may be deduced that for most energy efficient milling, the operation time may be chosen as 7 min.

Table 3.1- Concentration of copper and residue (non-metallic) in the milled samples after different milling time

S. N.	Sample time	Copper wt%	Residue wt%
1.	1.5 min	5.8	86
2.	7 min	21.9	74.6
3.	10 min	22.25	72.5

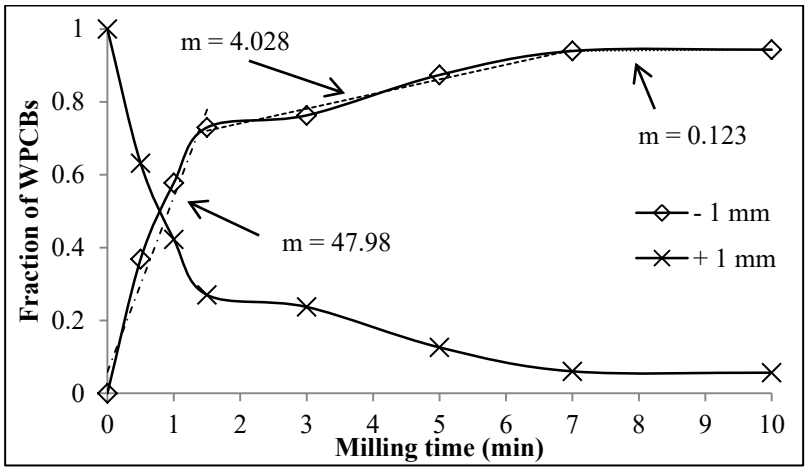

Figure 3.1- Distribution of WPCBs in –1 mm and +1 mm size at different milling time

3.1.2 Effect of feed rate on the milling of WPCBs

Increase in the feed rate of WPCBs from 3 $kg \cdot h^{-1}$ to 12 $kg \cdot h^{-1}$ showed 30 % reduction in the milling rates (**Figure 3.2**). This is because the increase in the feed rate results in more resistance to the movement of hammers and subsequently reduces the hammer's impact velocity. Further, higher feed rates also result in the distribution of exerted impact energy among more pieces of WPCBs, relatively. These forces may not be enough to prompt the brittle fracture, and thus the impact energy is absorbed by the

WPCBs pieces. The absorbance of impact energy not only deteriorates the milling rate but it may also result in the heating of WPCBs. Excessive heat may attribute to softening and sticking of WPCBs together, and it may lead to the breakdown of moving parts of the hammer mill. More temperature rise may also result in the decomposition of WPCBs and emission of toxic gases.

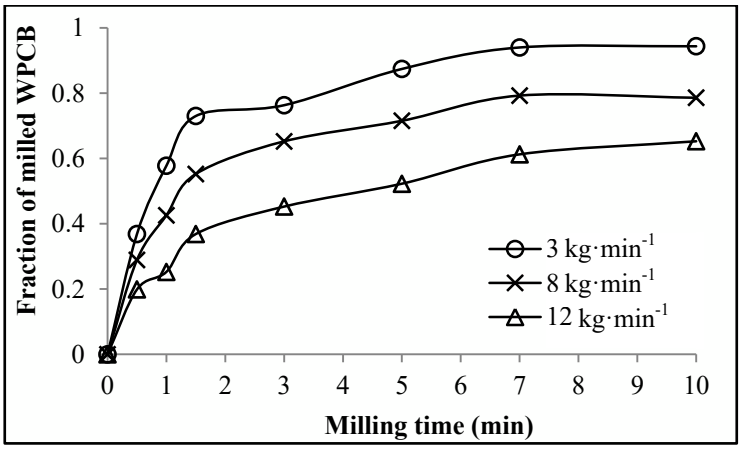

Figure 3.2- Amount of WPCBs milled to -1 mm at different feed rate

3.1.3 Sieve analysis of milled WPCBs

Sieve analysis of WPCBs particle crushed to –1 mm has been carried out to understand the size distribution pattern. Distribution of ground WPCBs in different size fractions is represented in **Figure 3.3** and it elucidates that the size distribution pattern of all particle follows a similar trend. This may be because the metal and nonmetal fraction obey a specific grinding behaviour during milling. It is evident from the curve that amount of ground WPCBs (-1 mm) in all size fraction increased by 2 – 3 times after 7 min milling compared to 30 sec. It is also found that 50 – 55 % of milled WPCBs are of +0.15 mm size, while particles of –0.15 mm size consist of 45 – 50 %.

Sieve analysis also showed that ground WPCBs are mostly concentrated in the –0.063 mm and –0.3 to +0.212 mm size fraction (**Figure 3.4**). Milling for 1.5 min resulted in

the concentration of 22.5 wt% particles in -0.063 mm size. Further, after 7 min milling, 30 % particles have been achieved–0.063 mm size and 17% particles attained –0.3 to +0.212 mm size.

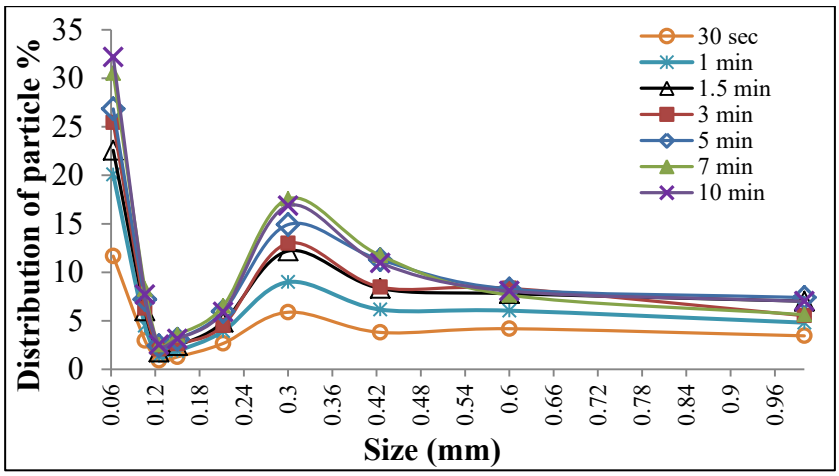

Figure 3.3- Particle size distribution of WPCBs powder (-1 mm)

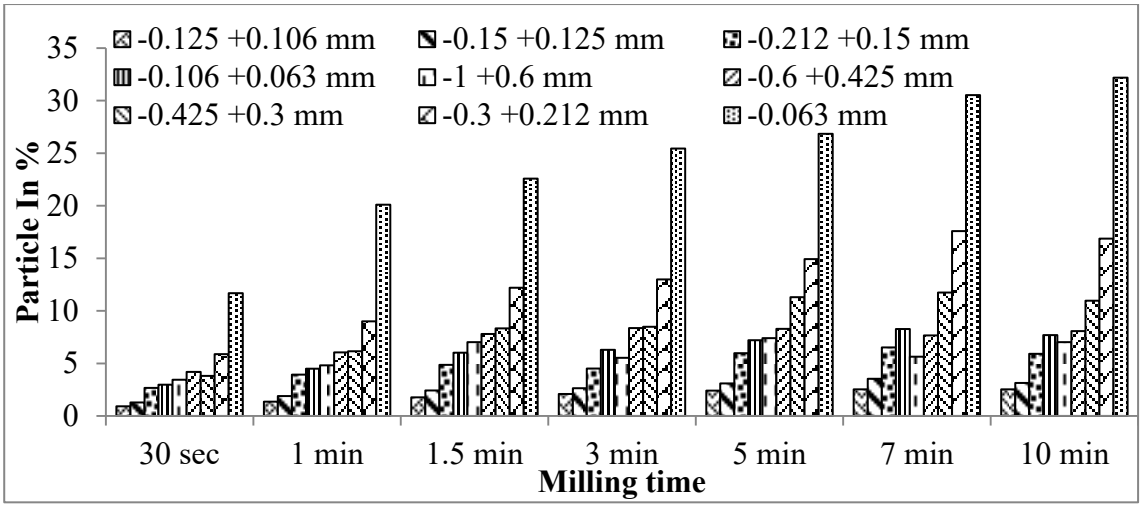

Figure 3.4- Distribution of crushed WPCBs in various size fractions at different milling time

3.1.4 Distribution of copper in different size fraction

The chemical analysis of ground WPCBs collected in various sieves has been carried out by AAS. The copper content in different size fraction after varying milling time is shown in **Figure 3.5.** Data reveals that coarser size fractions (+0.15 mm) are copper-

rich while the fine fraction is having copper content even less than 8%. It is because copper elongates during milling and could not be crushed to very fine size by the exerted impact forces. It has been found that nearly 75 – 80 % of the copper content of fed WPCBs is concentrated in +0.212 mm size after 7 min milling. Further, 83 – 87 % of the original copper content has been concentrated in the +0.15 mm size. Since, 50 – 55 wt% of milled WPCBs are in +0.15 mm size and thus, it can be interpreted from the data analysis that WPCBs of +0.15 mm comprise of nearly 43 wt% copper. Further, WPCBs of –0.15 mm size contains around 8 wt% copper only and rest non-metals.

From the above study, it has been found that copper present in WPCBs (22 wt%) may be enriched to 43 wt% with a recovery of ~87% in two steps *viz.,* milling of WPCBs to -1 mm size followed by sieving by using a sieve of aperture of 0.15 mm (ASTM 120).

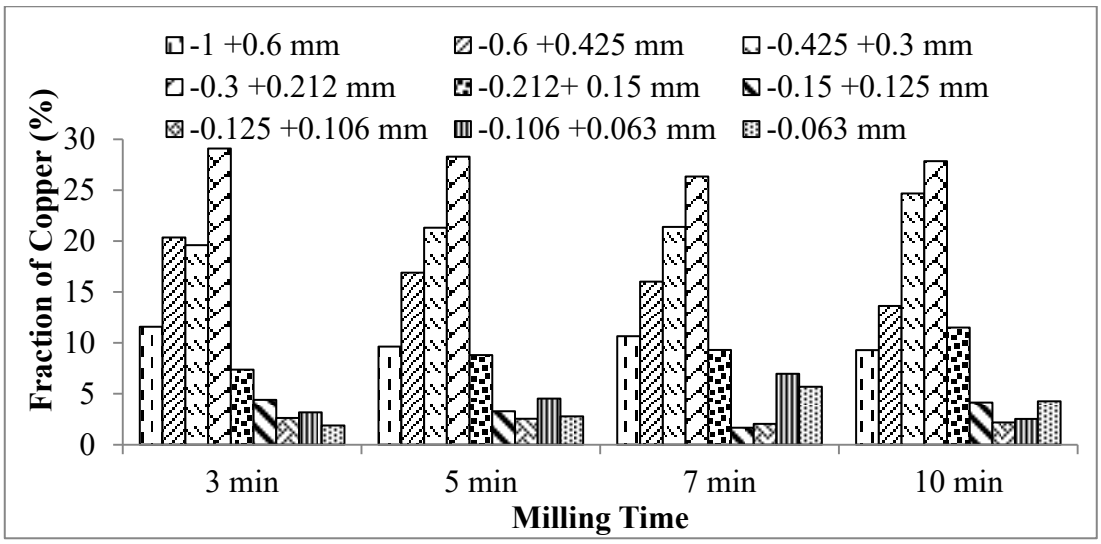

Figure 3.5- Distribution of copper in various size fractions of milled WPCBs after different milling time

3.1.5 Microscopic examination of milled WPCBs

Optical microscopic examination of milled WPCBs of – 1mm size at 10X magnification has been shown in **Figure 3.6**. The result shows that particles of copper, glass fibre and

non-metallic resin possesses different surface morphology and thus can be easily distinguished. During the milling, copper particles attain a flaky structure having reddish-brown lustre which is in resemblance to a torn thin film of copper. Glass fibre particles possess bamboo-like shape having fibrous morphology. On the other hand, the nonmetallic resin showed irregular polygon morphology with grey lustre.

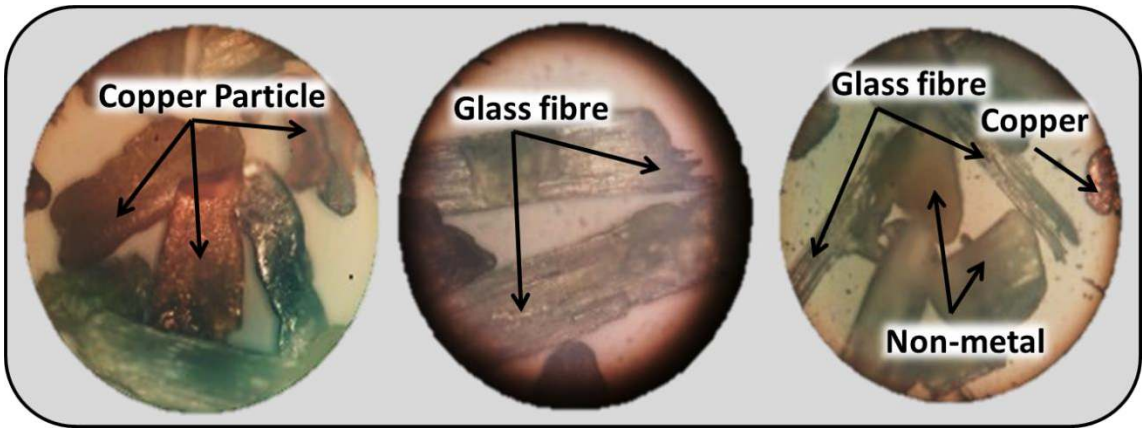

Figure 3.6- Copper, glass fibre and non-metallic particles in microscopic image of crushed WPCB (- 1 mm) after 7 minute

The SEM analysis of milled WPCBs (milling time-7 min) has been carried out and similar morphology has been as observed in **Figure 3.7** as seen in the optical microscopy. The EDS analysis of various particles showed varying compositions. It indicates that liberation of metal-nonmetal has been achieved after the milling. The glass fibre particle exhibits bamboo like fibrous structure and contains calcium, aluminium and silicon which are major constituents of glass-based material. On the other hand, a non-metallic particle having polygon shape showed the presence of a majority of carbon, oxygen and bromine. The non-metallic fraction apart from glass fibre is comprised of the HER and thus its EDS showed the presence of bromine and carbon. The copper particles are easily distinguishable in SEM due to their smooth

surface morphology. The EDS at a particular point showed a majority of copper confirming particle's identity.

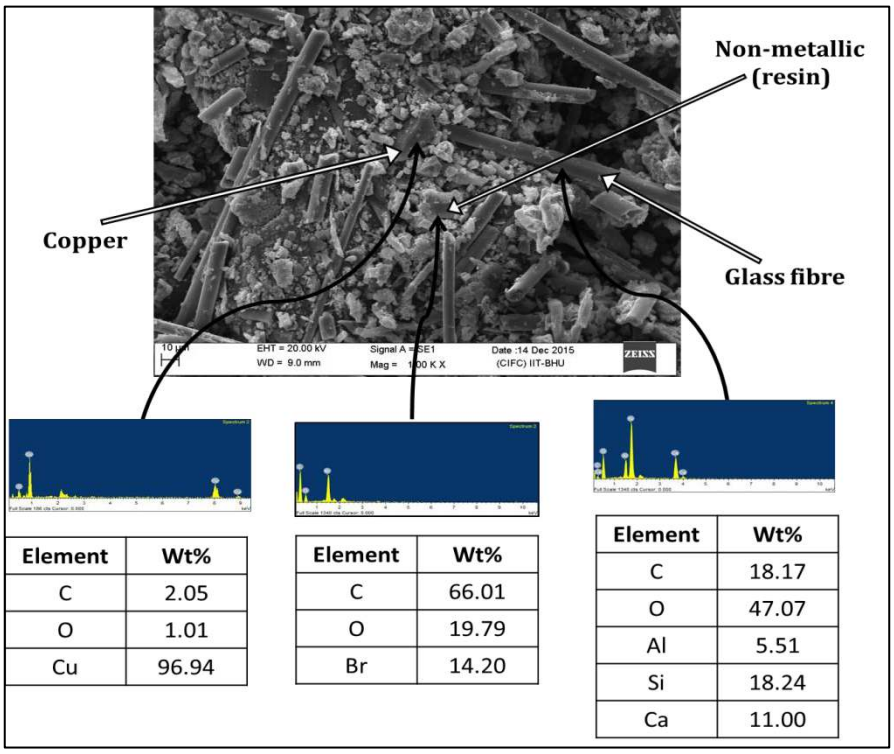

Element	Wt%
C	2.05
O	1.01
Cu	96.94

Element	Wt%
C	66.01
O	19.79
Br	14.20

Element	Wt%
C	18.17
O	47.07
Al	5.51
Si	18.24
Ca	11.00

Figure 3.7- SEM image of ground WPCBs after 7 min milling

Conclusions

Error! Reference source not found.**Figure 3.8** shows the graphical representation of the illing operation drawn from the present study. The same has been listed below:

- Optimization of operational parameters of hammer mill shows that milling rate of WPCBs is quicker initially (up to 1.5 min) and later slowed down and results in crushing of 94% feed after 7 min.
- After 7 min, no significant increment in the amount of crushed WPCBs has been registered.
- Sieve analysis showed that increase in milling time does not affect the size distribution pattern.
- After 7 min milling, the highest amount of crushed WPCBs were collected in –0.063 mm (31 wt%) and –0.3 +0.212 mm (18 wt%) size range.
- Nearly 50 – 55 wt% of WPCBs is milled to +0.15 mm size.
- Chemical analysis of ground WPCB after 7 min revealed that 83 – 87 % initial copper of WPCBs is concentrated in the +0.15 mm size.
- WPCB of +0.15 mm size contains 43 wt% copper and rest non-metal.
- Copper enrichment up to 43 wt% with ~ 87% recovery is achievable by sieving with a sieve of aperture 0.15 mm (ASTM 120)

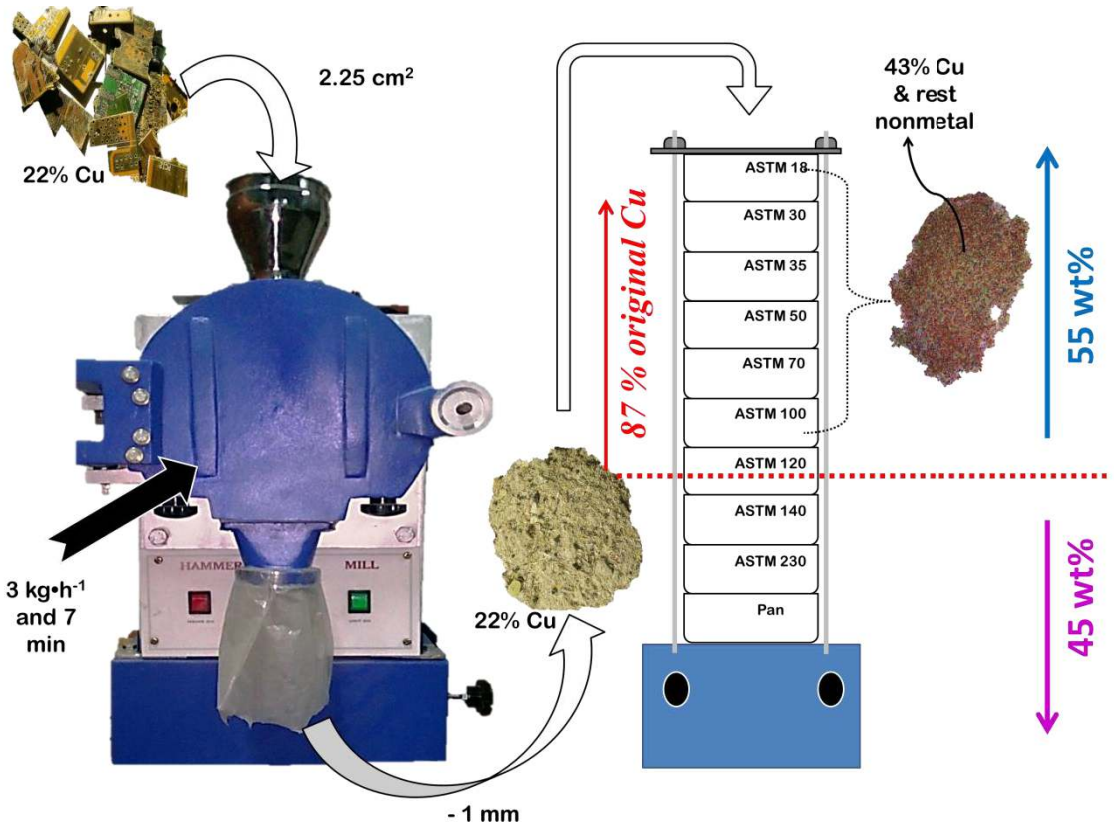

Figure 3.8- The graphical representation of the milling operation

Section- 2

Delamination of WPCBs by dissolution of HER in DMF

3.2 Delamination of WPCBs by dissolution of HER in DMF

The foray of HER dissolution in DMF showed anticipated results and thus, the effect of temperature, WPCB:DMF ratio (w/v; unit- $g \cdot mL^{-1}$), WPCBs size and time on dissolution leading to satisfactory dissolution and separation of components of WPCBs have been studied and discussed below.

3.2.1 Effect of temperature on HER dissolution in DMF

Effect of temperature (T) on the dissolution of HER has been studied in the range of 80 – 155 ^{o}C. **Figure 3.9** shows the efficacy of temperature on the dissolution of HER while other parameters were: WPCB:DMF ratio (weight/volume)- 1:10, time- 4 h, and WPCBs size- 4 cm^2. Initial delamination from the cross-section of WPCBs pieces has been observed after 30 min reaction irrespective of temperatures. Nature of curve reveals that the rate of HER dissolution in DMF increases up to 135 ^{o}C because of enhanced vibrations of rigid bonds of HER at elevated temperatures. The reversible breakage of van der Waals' bonds beyond glass transition temperature (T_g - 130 ^{o}C) [210] also promotes ease in bond formation between HER and DMF. After 4 h of reaction, nearly 0.79, 1.14, 0.91, and 0.43 $g \cdot L^{-1}$ of HER has been dissolved in DMF at temperatures 155, 135, 110, and 80 ^{o}C, respectively. At 155 ^{o}C, rapid decrease in the HER dissolution is observed. The fact behind is the operation close to the boiling point of DMF ($T_{B.P.}$= 153-154 ^{o}C) may lead to its decomposition [218,219,229]. Further, the temperature near T_{BP} may up-shoot the nucleation boiling; that triggers the localized evaporation of DMF resulting in reduced actual reagent availability during the experiment, although any vapour escaping out is condensed back.

The HER is the substrate that reinforces the different layers of copper tracks and glass fibre matrix together and thus HER dissolution results in delamination of WPCBs.

Thus, more dissolution of HER at elevated temperature is associated with more delamination (**Figure 3.10**). The progressing dissolution of HER through cross-section results in penetration of DMF inside the sandwiched structure of WPCB causing-swelling, cracking and separation of layers. The optimum temperature for maximum delamination of WPCBs has been found to be 135 ^{o}C at which the rate of dissolution of HER is highest. Notably, at 135 ^{o}C no gaseous pollutant is being generated because the decomposition of HER starts above 250 ^{o}C (please see the TGA analysis results discussed in **Section 2.3**).

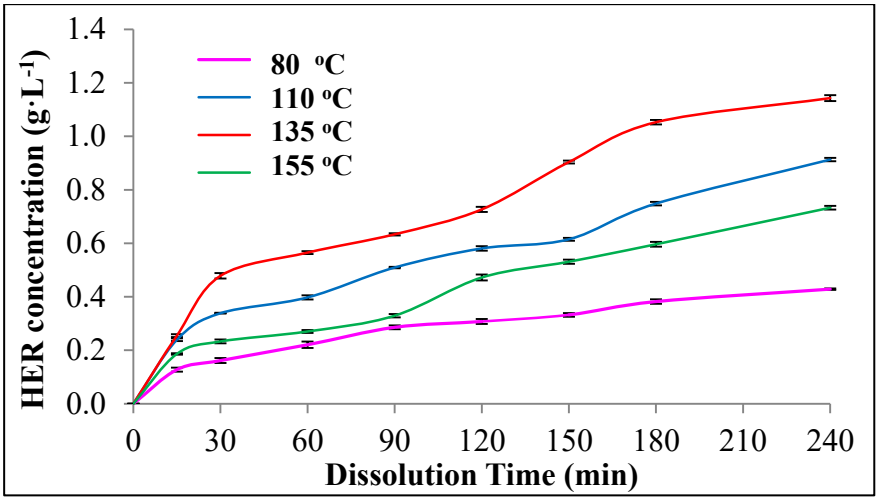

Figure 3.9- Effect of temperature on dissolution of HER
[WPCB:DMF- 1:10, 4 h, WPCB size- 4 cm^2]

3.2.2 Effect of WPCBs:DMF ratio on HER dissolution in DMF

The effect of WPCBs:DMF ratio on the dissolution of HER has been studied at 135 ^{o}C, for 4 h using WPCBs of 4 cm^2 and represented in **Figure 3.11**. The results show that small amount of HER dissolution is there at lower WPCB:DMF ratio. Further, it rises with an increase in WPCB:DMF ratios. The study revealed that at 0.5:10, 1:10 and 3:10 WPCB:PCB ratios nearly 0.53, 1.14 and 2.79 g·L^{-1} HER has been dissolved, respectively within 4 h reaction. At lower WPCB:DMF ratio less HER dissolution has been observed as a large proportion of solvent remains unutilized due to less solute

availability while an increase in WPCB:DMF ratio enables a high degree of solvent utilization.

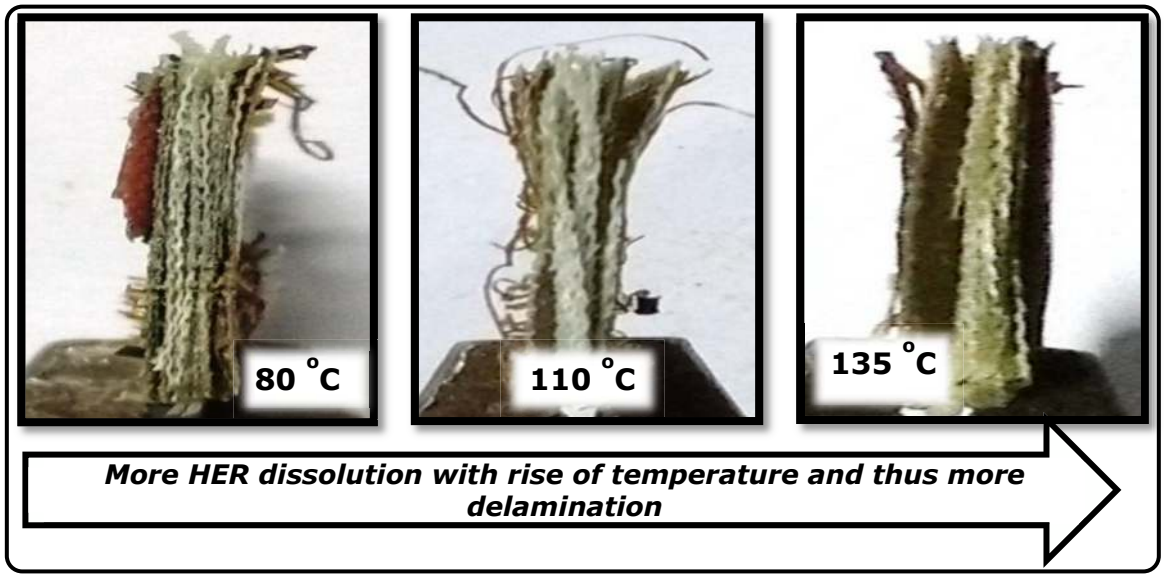

Figure 3.10- Improved delamination of WPCBs with rise in reaction temperature

This trend ceases to exist above WPCB:DMF ratio of 3:10 (i.e., 3.5:10 and 4:10) after 45 min reaction time. At 30 min, 0.84, 0.89 and 0.97 $g \cdot L^{-1}$ HER dissolution is seen at 3:10, 3.5:10 and 4:10 ratios, respectively. The reverse trend of HER dissolution has been observed later on. After 60 min, ~ 1.08 $g \cdot L^{-1}$ HER in DMF has been dissolved at 3:10 ratio, while 1.0 $g \cdot L^{-1}$ HER is dissolved in DMF at 3.5:10 and 4:10 ratio. This is because accelerated HER dissolution results in sufficient swelling of WPCBs that is capable of pushing many pieces out of the solvent pool. Thus, actual WPCB:DMF ratio falls below the pre-set value as well as below 3:10 after certain runtime. At WPCB:DMF ratio of 3.5:10 and 4:10 nearly 2.44 and 2.139 $g \cdot L^{-1}$ HER has been dissolved, respectively after 4 h. It is also noticeable that actual surface area of WPCBs exposed to solvent increased six times (26 cm^2 to 156 cm^2) once WPCB:DMF increased from 0.5:10 to 3:10. This indicates that surface area may affect the dissolution of HER from parent WPCBs. Based on the present study it may be deduced that WPCB:DMF

ratio of 3:10 has to be maintained for efficient HER dissolution, maximum delamination of WPCBs and most effective utilization of solvent. Results also indicated that the dissolution might be dependent on the DMF-WPCBs contact area.

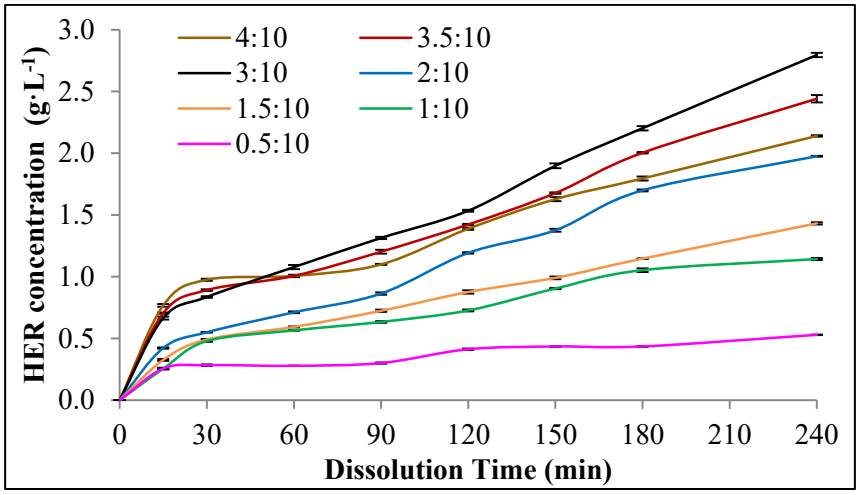

Figure 3.11- Effect of WPCB:DMF ratio on dissolution of HER

[4 h, 135 ^{o}C, WPCB size- 4 cm^{2}]

3.2.3 Effect of WPCBs size on HER dissolution in DMF

Study of variation of WPCB size from 16 cm^{2} to 1 cm^{2} at 135 ^{o}C and WPCB:DMF ratio of 1:10 shows that lower size results in quicker dissolution of HER, relatively (**Figure 3.12**). WPCBs of 16 cm^{2} showed 0.7 g·L^{-1} HER dissolution after 4 h which rose to 0.99, 1.14, and 1.68 g·L^{-1} as the WPCBs size reduced to 3, 2, and 1 cm^{2}, respectively. It is evident that size reduction of WPCBs pieces at fixed WPCB:DMF, does not alter the surface area but the exposed cross-sectional area of WPCBs to DMF is also increased. This indicates an important role of cross-section area in HER dissolution rather than surface area. Notably, at fixed WPCB:DMF ratio, 1 cm^{2} size pieces possess 4 times more cross-sectional area than WPCBs of 16 cm^{2} size. Further, chemically inert solder mask and copper tracks present on surface act as an obstacle in contact of solvent and HER beneath the surface. This also indicated that the surface area does not play an

important role in dissolution. It is thus inferred that rate of reaction of solvent along cross-sectional area is much faster than facial area. Further, as the delamination starts at the edge, solvent interlopes inside the layer of WPCBs to dissolve more HER (**Figure 3.13**). The visual observation of dried sample after treatment showed that 1 cm^2 size WPCBs have undergone very effective delamination. The size reduction below 1 cm^2 is difficult to get by a simple shear cutter, and it essentially requires a special type of automated equipment. Thus, the optimum WPCBs size of 1 cm^2 is chosen for further studies to ensure maximum dissolution of HER and the economy of the process.

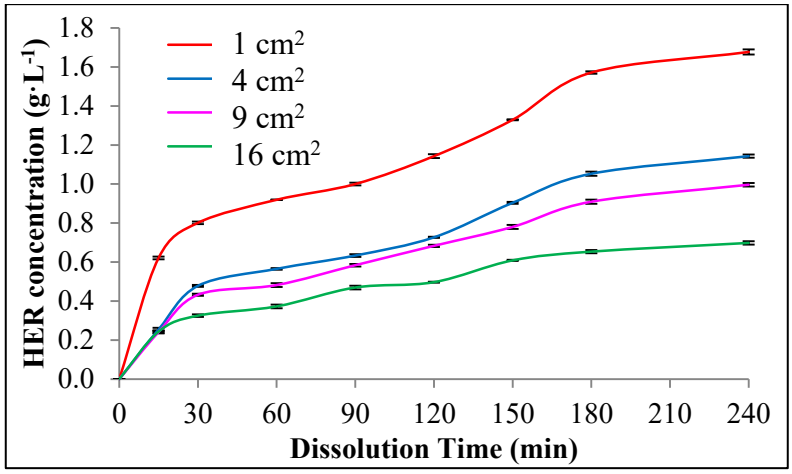

Figure 3.12- Effect of PCB size on dissolution of HER

[WPCB:DMF- 1:10, 4 h, 135 ^oC]

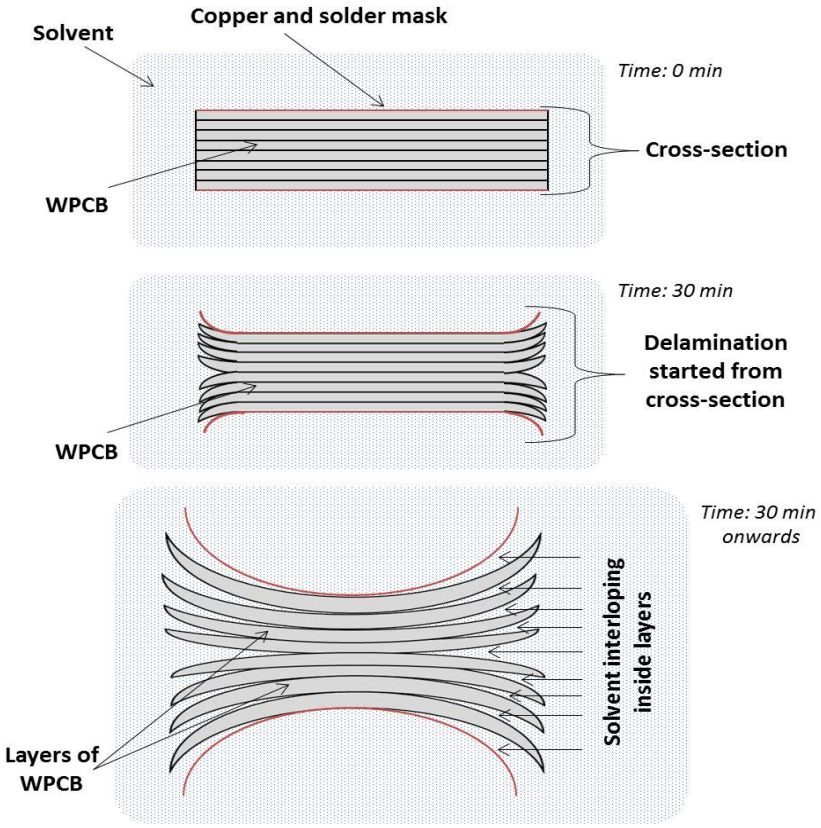

Figure 3.13- Representation of interaction of DMF on cross-section of WPCB

Thus, the optimum conditions found for most effective HER dissolution and subsequent delamination are: WPCB:DMF- 3:10, WPCB size- 1 cm^2, temperature- 135 ^oC.

3.2.4 Effect of time on HER dissolution in DMF

The effect of time on the dissolution of HER in DMF has been studied up to 60 h under optimum conditions *viz.* 135 ^oC, WPCB:DMF ratio- 3:10 and WPCBs size 1 cm^2 has been examined. The amount of HER dissolved at different time interval has been shown in **Figure 3.14.**

The nature of curve elucidates that up to 30 min, the rate of HER dissolution is relatively faster. This is because the DMF quickly dissolves HER from the cross-sectional area and later, hindered interloping of DMF inside the layers of WPCBs

occurs. This illustrated phenomenon has also been represented in **Figure 3.13**. It is also notable that under optimized conditions nearly 2.5 $g \cdot L^{-1}$ of HER has been dissolved in DMF after 4 h. The data also shows an increase in dissolution w.r.t time up to 48 h. Beyond 48 h, significant improvement in the dissolution of HER is not observed that indicates either saturation of DMF or complete dissolution of HER.

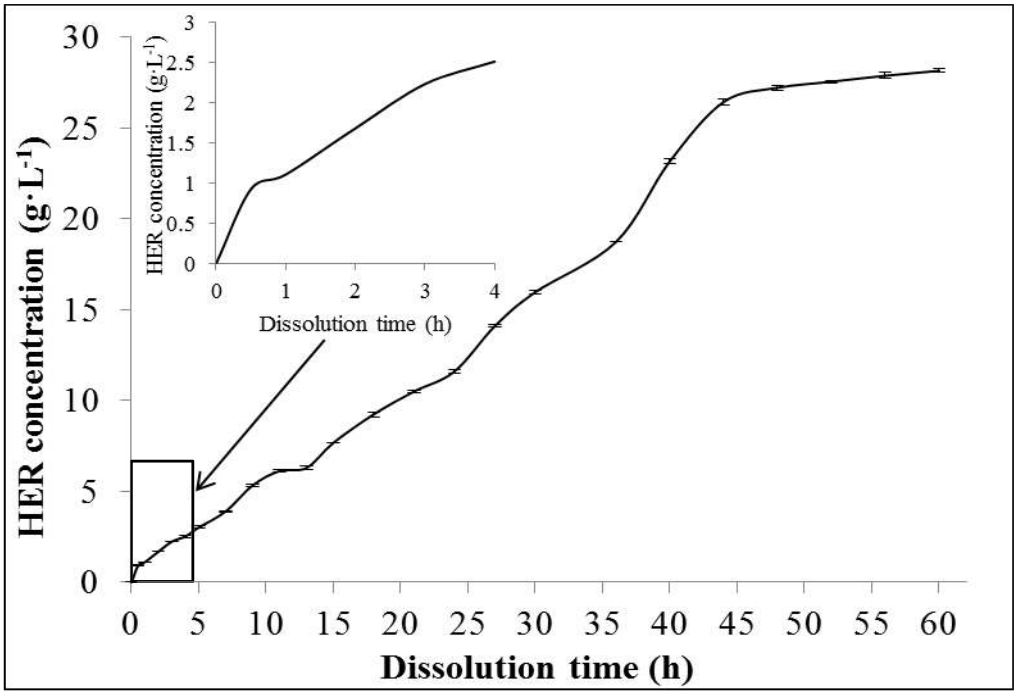

Figure 3.14- Effect of time on dissolution of HER in DMF
[WPCB:DMF- 3:10, 135 ^{o}C, WPCB size- 1 cm^2]

Results also showed that WPCBs of size 1 cm^2 has been separated into components *viz.,* glass fibre and copper foil after 150 min and solder mask after 240 min (**Figure 3.15**). The chemical analysis of the metal laminate liberated after treatment showed that it contains ~55% copper metal. This may be because, it is possible that copper laminate is separated yet some glass fibre, solder mask etc. are still adhered to it. The optimum processing time for most efficient delamination of WPCBs including the separation of the copper layer has been observed to be 4 h in the present study. Although depending upon post-processing techniques, different times may be chosen. For example, the

WPCBs treated for 48 h are having low HER content, and thus its thermal processing will emit extremely low dioxins and furans.

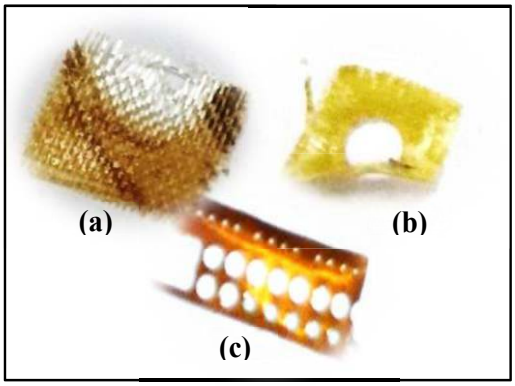

Figure 3.15- Separated components of WPCB (a) glass fibre (b) solder mask (c) copper laminates

3.2.5 Recovery of spent DMF by regeneration

After the reaction, the pregnant DMF having yellowish appearance has been recovered by filtration (**Figure 3.16**). The pregnant DMF has been regenerated producing a colourless liquid having an appearance similar to original DMF (**Figure 3.16)**. The DMF is a commercial solvent having the potential of recycling, and thus in-depth study has been carried out to verify the possibility of its recycling after treatment. Therefore, the chemical composition and molecular structure of regenerated liquid have been examined by different techniques.

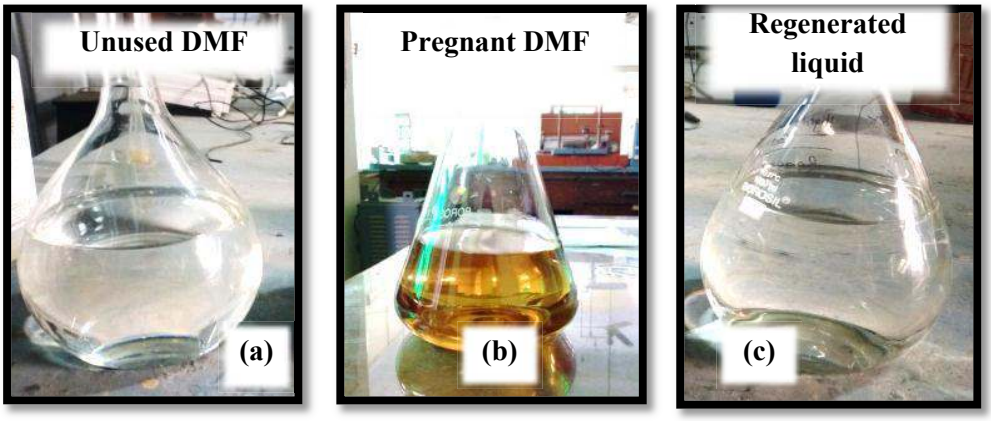

Figure 3.16- (A) Unused DMF, (B) pregnant DMF, and (C) Regenerated liquid

The NMR analysis has been performed to understand the respective positions of hydrogen and carbon moieties. The ^{1}H-NMR, as well as ^{13}C-NMR spectra of unused DMF, and regenerated liquid are similar showing that the respective position of hydrogen and carbon atoms after regeneration is unaltered. This also indicates that no impurities are being associated with regenerated liquid. The unused DMF and regenerated liquid showed a ^{1}H-NMR signal at 8.01, 2.9, 2.8 ppm (**Figure 3.17-A**) and the ^{13}C-NMR signal at 161.6, 35.5, 30.4 ppm (**Figure 3.17-B**), respectively. The obtained NMR spectra are identical to standard proton and carbon chemical shift spectra of pure DMF [230,231]. Based on the above study a fact may be established that spent DMF can be recycled with very high purity.

The FT-IR analysis of unused DMF and regenerated liquid has also been carried out to find out their respective molecular structure. The analysis showed similar spectra for both systems as shown in **Figure 3.18**. The spectral analysis showed vibrations corresponding to C-H stretch of alkanes at 3000-2850 cm^{-1}, C=O stretch (1670 cm^{-1}), C-N stretch (1250-1020, 657 cm^{-1}). These bands are identical to the FT-IR spectra of pure DMF reported in the literature [230,232]. The FT-IR analysis results also corroborate the NMR analysis results. The NMR and FT-IR analysis validated that regenerated liquid is DMF. Recycling of DMF with high purity ensures clean, cost-effective, and negligible effluent generating operation.

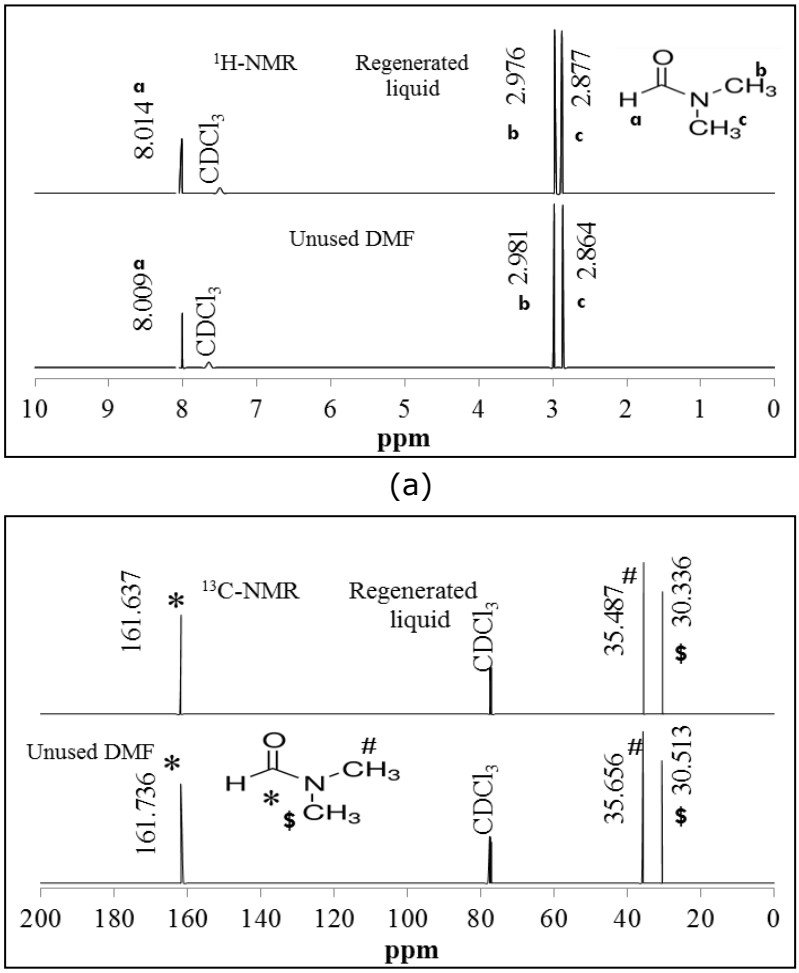

Figure 3.17- (A) ^{1}H-NMR (B) ^{13}C-NMR spectra of unused and regenerated DMF

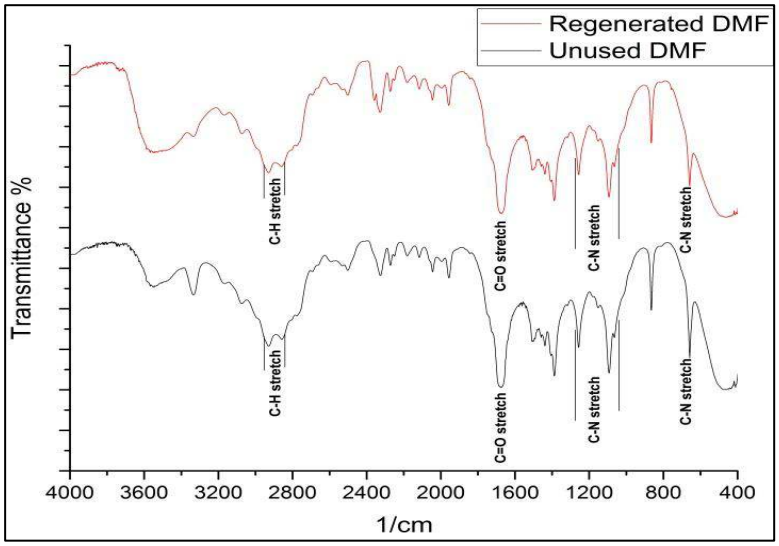

Figure 3.18- FT-IR spectra of unused and regenerated DMF

3.2.6 HER dissolution efficiency of regenerated DMF

The regenerated DMF has been used to treat WPCBs five times under optimized condition *viz.* 135 ^{o}C, WPCB:DMF ratio- 3:10, WPCB size- 1 cm^2, and 4 h. After each dissolution cycle, spent solvent was regenerated and used for the treatment of WPCBs in next cycle. The average quantity of dissolved HER in five cycles has been represented with standard deviation bars in **Figure 3.19**. It may be interpreted from data that, capabilities of DMF to dissolve HER after five cycles are equivalent to pure and unused DMF.

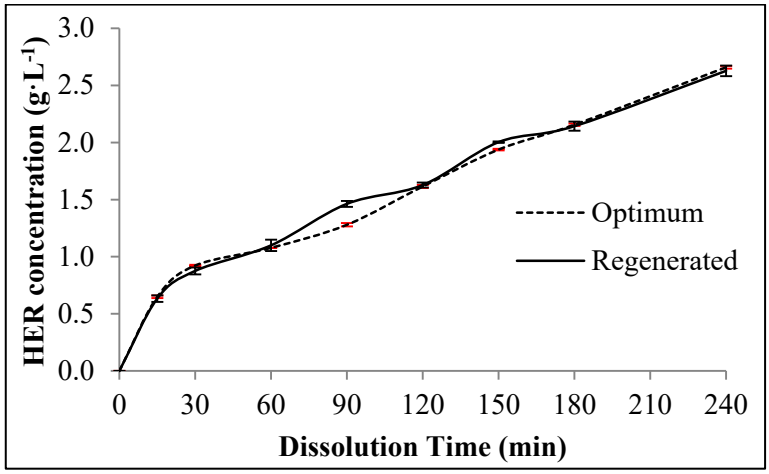

Figure 3.19- Dissolution of HER in fresh DMF and five times regenerated DMF [WPCB:DMF- 3:10, 4 h, 135 ^{o}C, WPCB size- 1 cm^2]

3.2.7 Analysis of recovered residue obtained after regeneration

The interaction of DMF with WPCB showed the dissolution of HER and recycling of consumed DMF. On the basis of this, an analogy may be assumed that the recovered residue after regeneration of DMF is HER and other polymeric material. To study the morphology and quantitative composition of the residue and untreated HER, SEM-EDS has been carried (**Figure 3.20).** It is evident that morphology of untreated resin is slightly diverse than residue due to non-uniformly distribution and adhered nature of

HER particles. The residue particle exhibits polygon morphology having non-adhered structure. The EDS analysis revealed that residue as well as untreated HER contain carbon, bromine, and oxygen only.

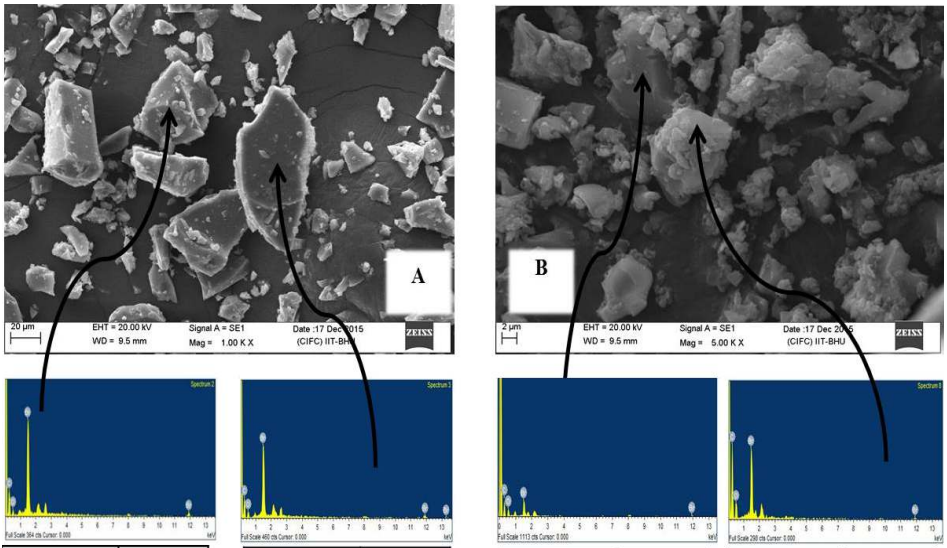

Element	wt%
C	63.49
O	8.97
Br	27.53

Element	wt%
C	62.75
O	12.12
Br	25.13

Element	wt%
C	56.32
O	29.82
Br	13.86

Element	wt%
C	65.67
O	19.31
Br	15.01

Figure 3.20- Morphology and elemental composition of (A) residue and (B) untreated HER

Although the similarity in composition and slight variation in the morphology shows an agreement with the proposed analogy yet, it does not give a determinant conclusion. Thus, investigations were extended, and FT-IR spectra of pure BPA, residue, and untreated HER have been recorded. The FT-IR spectra of pure BPA, residue and untreated HER is shown in **Figure 3.21.**

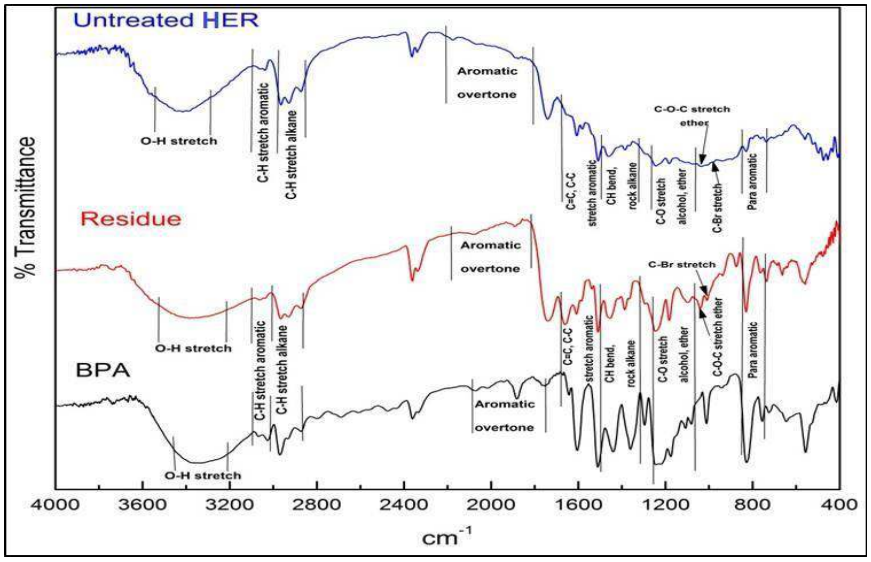

Figure 3.21- FT-IR spectra of pure BPA, residue, and untreated BPA

The analysis showed vibrations corresponding to stretching bands of O-H and C-O of alcohol, C-H of aromatic and alkane, C=C and C-C of the ring. Vibrations for aromatic overtones, bending and rocking of alkane, and para distributed aromatic are also present in pure BPA, residue, and untreated HER. Additionally, vibration corresponding to C-Br stretch, and C-O-C stretch of ethers have also been identified in residue and untreated HER (except BPA). This is because HER is formed by polymerization of bromine substituted BPA using ethers as a linkage [223,224]. The peak values corresponding to vibrations of the various functional group is indexed in **Table 3.2** [230,232–234]. The FT-IR data confirms the presence of the major constituent of HER (phenol, alcohol, hydroxyl, ether group etc.) in the residue; that corroborates the results found by SEM-EDS analysis. The SEM-EDS and FT-IR analysis confirm the analogy that residue recovered after the regeneration is HER. Therefore, the separation of HER from parent WPCBs and its recovery as residue ensures its safe disposal.

Table 3.2- Peak spectra of various bands in FT-IR spectrum

Functional group	Peak (cm^{-1})	Pure BPA	Untreated HER	Residue
O-H stretch (alcohols)	3355-3250	✓	✓	✓
C-H stretch (aromatic)	3060-3025	✓	✓	✓
C-H stretch (alkane)	2970-2870	✓	✓	✓
Aromatic overtone	2970-2870	✓	✓	✓
C-C, C=C stretch in rings	1680-1510	✓	✓	✓
C-H bend & rock	1460-1360	✓	✓	✓
C-O stretch (alcohol, phenol)	1294-1070	✓	✓	✓
C-Br stretch	1028-1009	×	✓	✓
Para distributed aromatic	875-660	✓	✓	✓
C-O-C stretch (ether)	1040	×	✓	✓

3.2.8 Chemical Interaction

The chemical structure of DMF is shown in **Figure 3.22** along with the present hydrogen bonding moieties. The availability of 3 hydrogen bond donor sites makes DMF a good solvent. It readily dissolves many organic compounds due to the formation of the hydrogen bond. Hydrogen of C-H group of DMF is a major hydrogen bond donor site [235]. Further, the presence of nitrogen atom also enhances the hydrogen bonding capabilities [207]. However, the full chemistry of DMF-HER interaction is not explored presently and needs further investigation. Factors like- rupture of van der Waals' bonds at high temperature, the moderate vibration of HER bonds, and strong H-bonding affinity of DMF indicate towards the fact that hydrogen bonding between WPCBs and

DMF is responsible for the dissolution of HER. Further, recovery of HER and unaltered chemical structure of DMF after regeneration also point towards simple solvation of HER instead of the molecular exchange reaction. Thus, possible hydrogen bonding interaction of DMF and HER is represented in **Figure 3.23** and explained. **Figure 3.23-A** shows the formation of hydrogen bond between the nitrogen atom of DMF and hydroxyl group, due to pulling of the hydrogen atom by the strong electronegative nitrogen. The electrostatic force exerted due to pulling of the electron by hydrogen of the hydroxyl group of HER towards oxygen molecule of DMF may attribute to H-bonding (**Figure 3.23-B**). The hydrogen atom of the methyl group of DMF may participate in H-bonding with bromine and oxygen neighbouring the aromatic chain of HER (**Figure 3.23-C**).

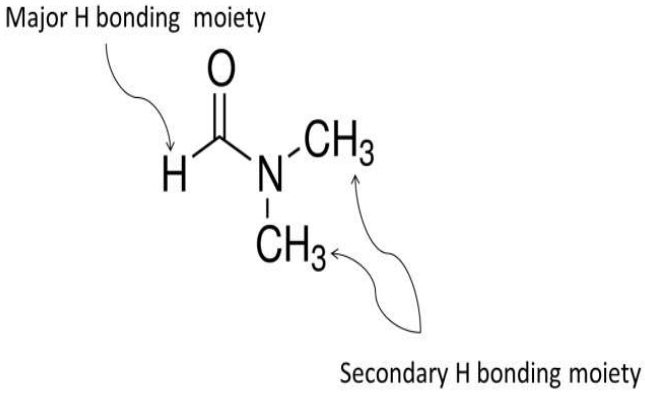

Figure 3.22- Chemical structure of DMF and its hydrogen bonding moieties

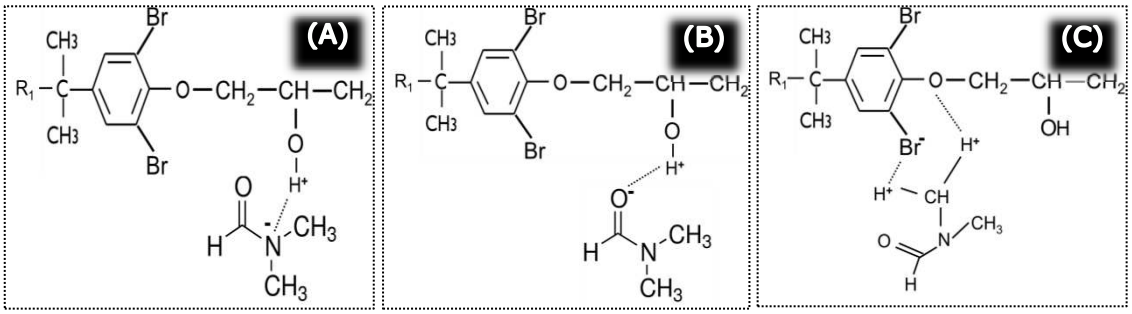

Figure 3.23- Hydrogen bond interactions resulting dissolution of HER into DMF

The overall flow sheet of the proposed process may be represented as shown in **Figure 3.24**. The beauty of the investigated process is: (a) recycling and reuse of spent DMF, and (b) recovery of HER and its safe disposal. Thus, treatment of WPCBs by DMF has proven to be an effective way ensuring delamination of WPCBs and dissolution of HER. A few factors like regeneration of DMF, negligible drop in HER dissolution efficiency after regeneration, recovery of dissolved HER as residue etc. make this process very cost effective, environment-friendly and low effluent generating.

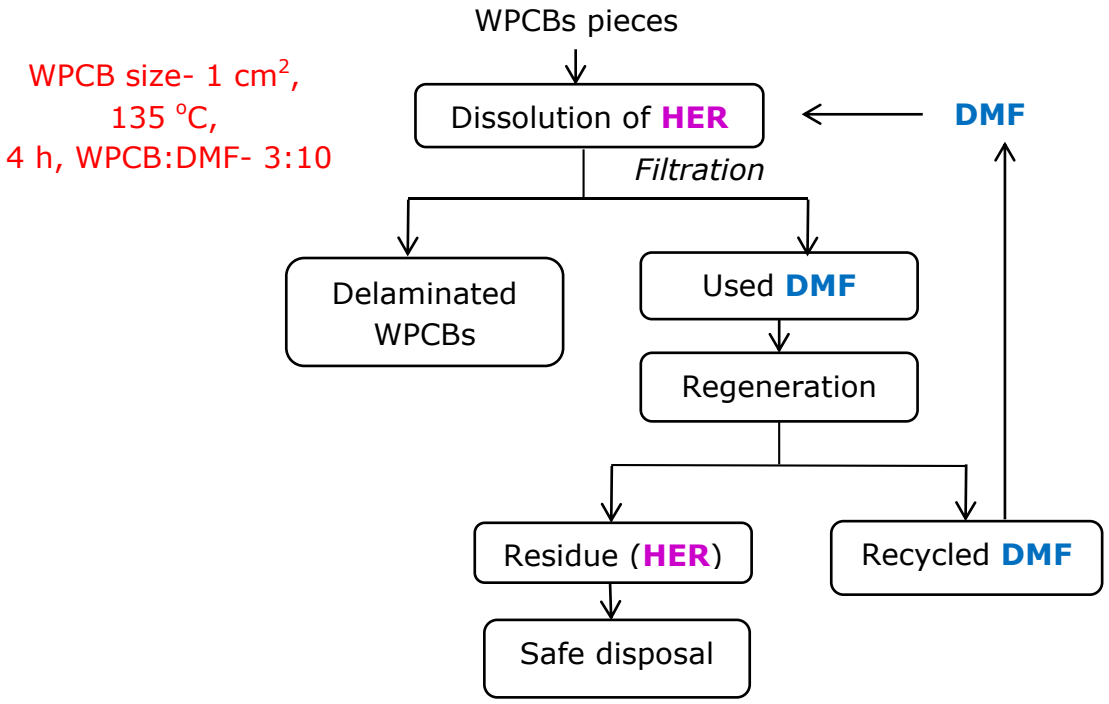

Figure 3.24- Flow sheet of the proposed process for dissolution of HER by using DMF

Conclusions

The investigation and results illustrated that HER could be successfully dissolved in DMF to achieve significant delamination of WPCBs. The various important points relevant to the present study are listed below:

- Optimized parameters for efficient HER dissolution are: 135 ^{o}C, 4 h, WPCB:DMF-3:10 (w/v) and fed WPCB size of 1 cm^{2}
- Under optimized parameters, 2.5 g·L^{-1} of HER has been dissolved in DMF and complete separation of glass fibre matrix, solder mask, and copper laminate is achieved
- The solvent reacts along the cross-section of WPCB pieces at very faster rates compared to its action on surface
- After usage, spent DMF can be easily recycled with high purity and without significant loss in the HER dissolution capabilities
- The dissolved HER in DMF is also recovered as residue, and thus it may be disposed off properly
- The results and various factors observed during the study indicated that hydrogen bonding might be the phenomenon responsible for HER dissolution.

Section- 3

Liberation of WPCB's metal-laminates by HER dissolution using DMA

3.3 Liberation of WPCB's metal-laminates by HER dissolution using DMA

The previous section embodies the utility of solvent DMF for HER dissolution and delamination of WPCB. Present section exemplifies the dissolution behaviour of HER and liberation of metal clad of WPCBs in solvent DMA. The solvent DMA also belongs to amide group and owns structural similarity with DMF. In DMA, methyl (CH_3) group is linked to the carbonyl (C=O) moiety in place of hydrogen molecule of DMF. Due to the difference in the chemical structure, DMA possesses high molar volume, boiling point, heat capacity, and dipole moment (**Chapter 2, Table 2.1**). Preliminary trails by using DMA showed positive results, and thus experiments at varying WPCB:DMA ratio, temperature, time and WPCB size have been performed. The results obtained are presented and conferred below:

3.3.1 Effect of HER dissolution at different temperatures

The efficacy of HER dissolution in DMA has been studied at different temperatures *viz.,* 120, 140 and 160 ^{o}C as shown in **Figure 3.25**. The HER dissolution follows the similar trend as registered in case of solvent DMF, i.e., the increase in temperature favours the dissolution. At 120 ^{o}C, after 4 h only 1.3 g·L^{-1} HER has been dissolved which rose to 2.0 g·L^{-1} and 2.6 g·L^{-1} as the temperature increased to 140 ^{o}C and 160 ^{o}C, respectively. It may be attributed due to reversible rupture of internal van der Waals' bonds above T_g of WPCBs. The experiments beyond 160 ^{o}C were not performed as it may lead to decomposition of DMA. Similar to DMF, DMA dissociation may also start near its boiling point (164– 165 ^{o}C) that in turn will result in low HER dissolution [221]. The data also shows that the HER dissolution is quick up to 15 min and later it is slowed down. This indicates quicker reaction rates compared to DMF which shows similar trend up to 30 min behaviour. The **Figure 3.26** shows that more dissolution of HER

with time results in more delamination of WPCBs. It is also evident that at 160 ^{o}C, almost complete delamination of WPCBs occurs after 3 h. Prolonged contact with DMA at high temperature also dissolves the 'Solder mask'. It ensures the maximum exposure of copper clad to lixiviate is during post-hydrometallurgical treatment. The study shows that in 3 h time, 2.5 g·L^{-1} HER has been dissolved and successful delamination of 1 cm^2 size WPCBs is achieved.

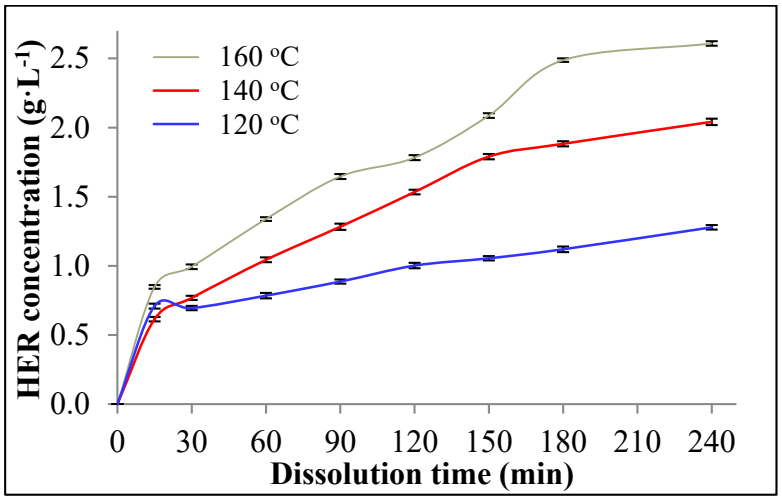

Figure 3.25- Effect of temperature on dissolution of HER at different time [WPCB:DMA- 3:10, 4 h, 1 cm^2]

3.3.2 HER dissolution at varying WPCB:DMA ratios

Based on the observation in case of DMF, experiments at 1:10, 2:10, and 3:10 WPCB:DMA ratios have been executed using DMA. Variation of WPCB:DMA ratio showed similar results as found in case of solvent DMF. The WPCB:DMA ratio of 3:10 has been the limiting ratio because higher ratio promotes rejection of WPCB from the solvent pool due to excessive swelling (discussed in **Section 3.2.2).** The result shows that higher WPCBs concentration in solvent led to more dissolution of HER as seen in case of DMF (**Figure 3.27**). It is due to increased availability of HER, and greater utilization of DMA at high WPCB:DMA ratios. Data reveals that with an increase of

WPCB:DMA from 1:10 to 3:10, HER dissolution rose to 2.6 $g \cdot L^{-1}$ from 1.0 $g \cdot L^{-1}$ after 4 h.

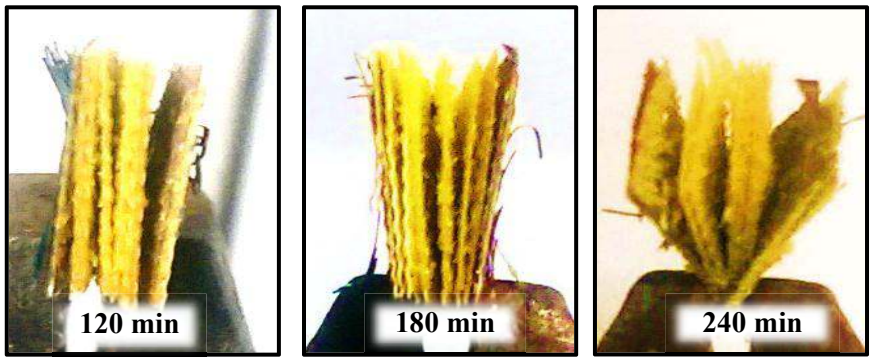

Figure 3.26- Digital photographs of WPCBs at different time
[WPCB:DMA- 3:10, 160 °C, WPCB size- 1cm^2]

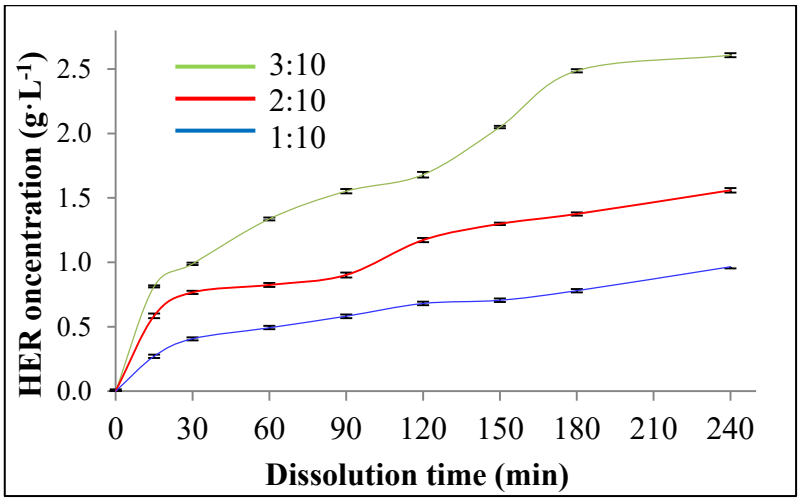

Figure 3.27- Effect of WPCB:DMA (wt/vol) ratio on dissolution of HER at different time
[4 h, 160 °C, WPCB size- 1 cm^2]

The HER reinforces the WPCB structure, and thus, it's dissolution attributes to cracking and liberation of layers of WPCBs. Observation showed that at WPCB:DMA ratio of 3:10 and 160 °C, complete delamination has been achieved in 3 h. Further, along with the HER, dissolution of inert solder mask has also been observed in all experiments w.r.t. time (**Figure 3.28**). Almost complete solder mask dissolution has been registered after 4 h time for 1 cm^2 WPCBs. It is noteworthy that solvent DMA is

capable to dissolves solder mask while DMF resulted in the separation of solder mask after treatment.

Figure 3.28- Dissolution of solder mask after different time [WPCB:DMA- 3:10, 160 ^{o}C, WPCB size- 1 cm^2]

3.3.3 Liberation of metal laminates of WPCBs of varying size

Effect of dissolution of HER from different size WPCBs showed the reciprocal relationship between the size and dissolution rate (**Figure 3.29**). As the WPCB size increased from 1 cm^2 to 9 cm^2, almost 40% drop in HER dissolution has been encountered. It is also evident from the nature of curve (corresponding to WPCB of size 1cm^2) that up to 15 min, the rate of reaction of DMA is very fast (slope = 0.06 g·L^{-1}·min). Later, the rate of reaction is slowed down up to 3 h (slope = 0.01 g·L^{-1}·min), and beyond 3 h the slope is close to zero. It indicates that dissolution rate of HER after 180 minutes is extremely slow, and the maximum amount of HER has dissolved up to 180 min at 3:10 ratio of WPCB:DMA and 160 ^{o}C. This is caused because large size pieces exert lower specific cross-sectional area and thus retards the rate of HERS dissolution (please see **Chapter 3, Section 3.2.3** for details). Another reason may be the presence of more number of '*through holes'* on large size WPCBs (please see **Chapter 1, Section 1.8** for details about the role of '*through holes'* in WPCBs). These holes are usually coated with electrolytic copper that remains firmly attached to its wall as shown

in **Figure 3.30**. Since DMA doesn't react with copper laminate thus even after the significant dissolution of HER, copper inside through holes keeps the layers sticking together and also hinders in the interloping of DMA to the nearby area.

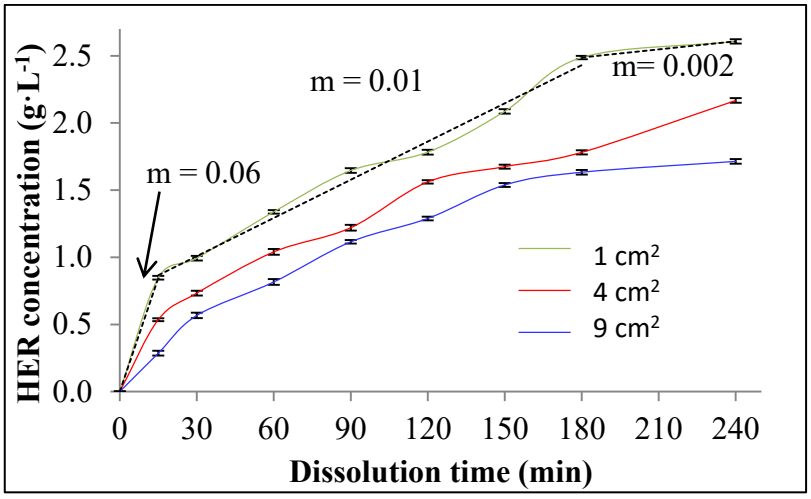

Figure 3.29- Effect of fed WPCB size on dissolution of HER

[WPCB:DMA- 3:10, 160 ^{o}C, 4 h]

From the above studies it has been found that maximum HER dissolution resulting in the satisfactory delamination is achieved under conditions *viz.,* WPCB:DMA- 3:10, 3 h, 160 ^{o}C and 1 cm^{2} WPCBs. After delamination of the metal laminate, glass fibre matrix was also separated and the chemical analysis of metal laminates showed the presence of ~ 80% copper. This indicates that even after detachment from parent WPCBs some glass fibre, epoxy resin, or small quantity of solder mask are still adhered. The separated components of WPCBs after treatment are also shown in **Figure 3.31**.

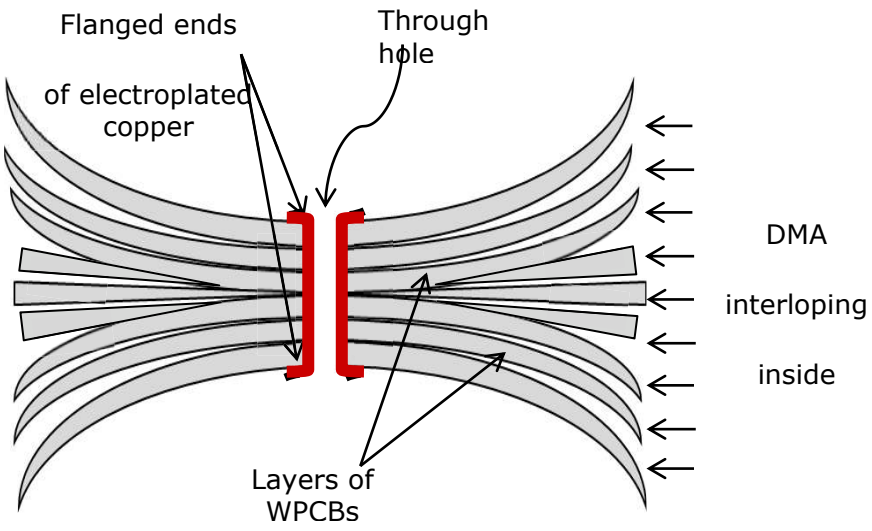

Figure 3.30- Schematic view of through holes that hinders the easy liberation of WPCBs layers

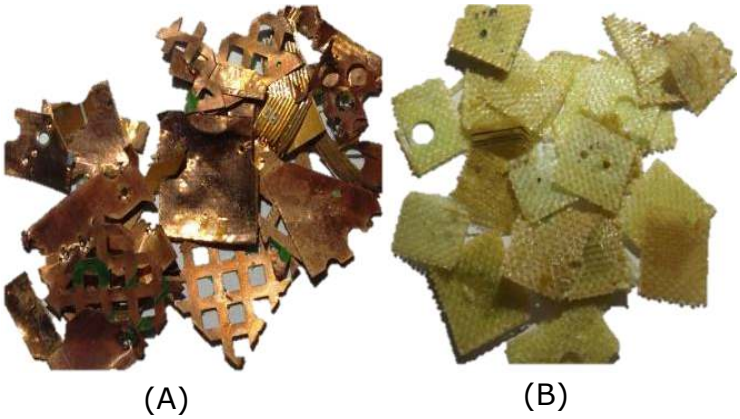

Figure 3.31- Components of DMA treated WPCBs (A) copped laminates and (B) glass fibre matrix

3.3.4 Investigation regarding recycling of spent DMA

After the dissolution, the pregnant DMA has been collected separately by filtration and then subjected to regeneration. The pregnant DMA possess different colours i.e. red, yellow, green, brown etc. unlike the pure and regenerated liquid which is colourless (**Figure 3.32**). The different colours are seen due to the dissolution of solder mask in DMA because solder mask's colour varies from manufacturer to manufacturer. An in-

depth study has been carried out to investigate the physical properties, chemical structure, and thermal decomposition behaviour of regenerated liquid.

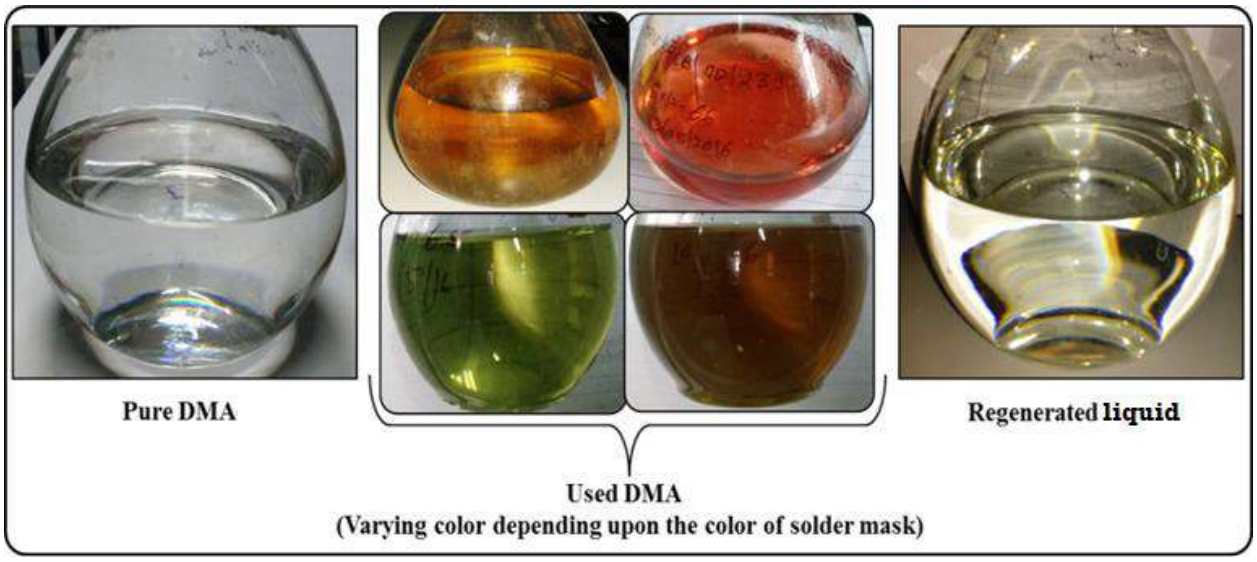

Figure 3.32- Physical appearance of pure DMA, used DMA and regenerated liquid

The initial boiling point of the regenerated liquid has been measured by 'ASTM D86' standard. It has been found to be 165 ^{o}C that is in the range of boiling point of pure DMA (164 – 165 ^{o}C).

The ^{1}H-NMR and ^{13}C-NMR analysis of regenerated liquid has been performed to understand the molecular arrangement and obtained spectra are shown in **Figure 3.33** and **Figure 3.34**, respectively. Spectral analysis revealed that regenerated solution exhibits signals for hydrogen and carbon atoms identical to the pure DMA [231]. The hydrogen atoms of the methyl group in conjugation with nitrogen have shown signals at 3.033 and 2.933 ppm, respectively. The hydrogen atom nearby the carbonyl group has shown a signal at 2.077 ppm. The carbon atoms of the methyl groups attached to nitrogen have shown signals at 37.683 and 34.730 ppm, respectively. Carbon atoms present in the carbonyl group and methyl group adjacent to carbonyl moiety have shown signals corresponding to 170.228 ppm and 21.178 ppm, respectively. The similarity of

NMR data of regenerated liquid to pure DMA revealed that regeneration doesn't alter the chemical structure of DMA and thus, vanishes the need of fresh DMA. Further, the regenerated liquid does not have different NMR signal rather than pure DMA, indicating the success of regeneration process with extreme purity.

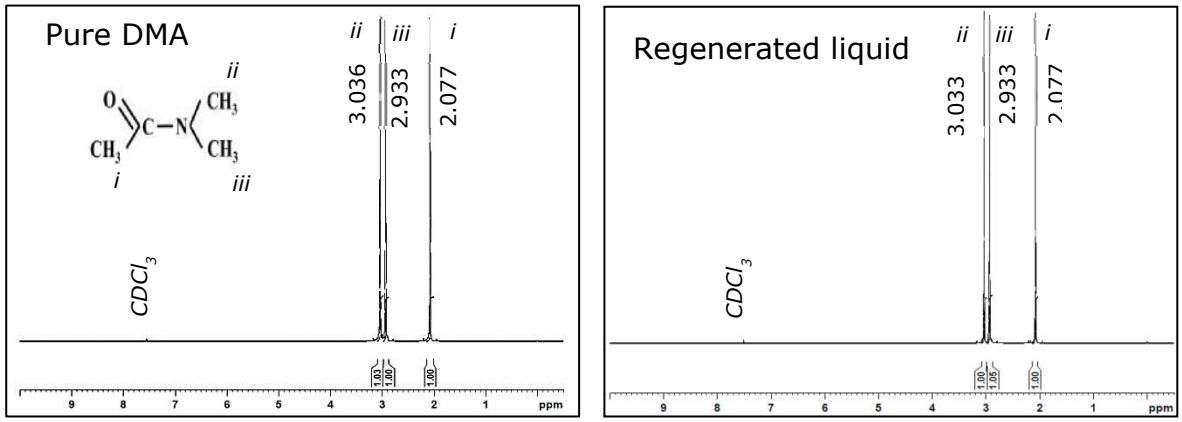

Figure 3.33- ^{1}H-NMR spectra of pure DMA and regenerated liquid

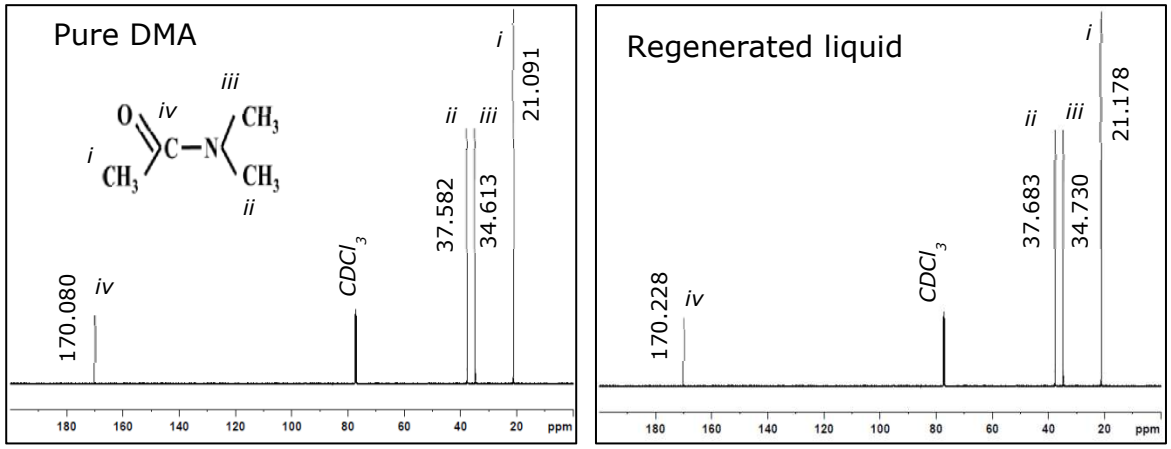

Figure 3.34- ^{13}C-NMR spectra of pure DMA and regenerated liquid

The FT-IR spectrum has been recorded to understand the molecular structure of regenerated liquid and pure DMA. Similar vibrations bands have been found to exist in the FT-IR spectra of pure DMA and regenerated mass. Both spectra (**Figure 3.35)** have shown vibrations corresponding to C-H, C=O and C-N stretch as well as C-H bending and C-(CH_3) rocking.

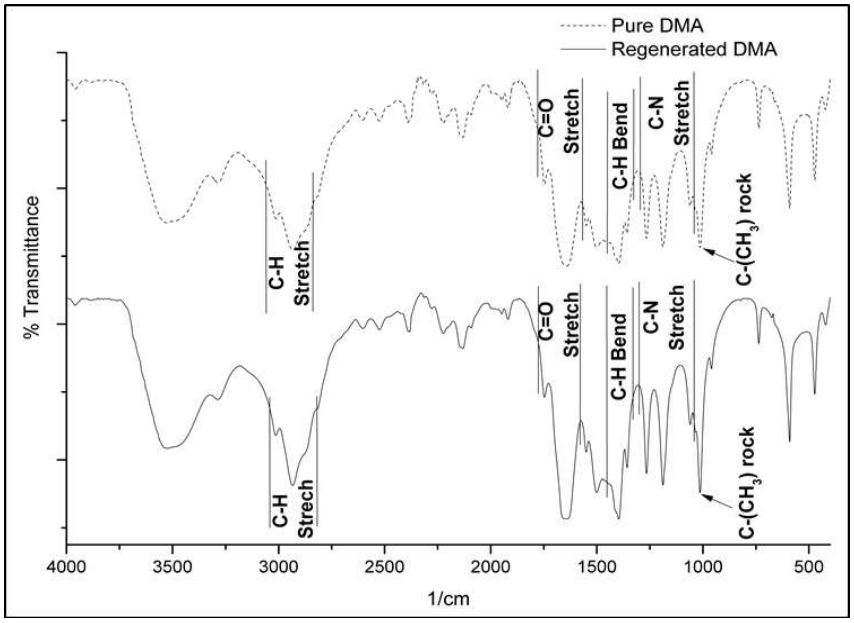

Figure 3.35- FT-IR spectrum of pure and recycled DMA

The peak values corresponding to the different functional groups are listed in **Table 3.3**. The FT-IR confirms the presence of methyl, carbonyl, amide functional groups which are the major constituents of pure DMA also and thus, corroborates the results obtained by NMR analysis.

The thermal stability of regenerated liquid has been examined by TGA-DTG, and obtained results are compared with pure solvent. The TGA-DTG data plots of both systems were found alike and have been presented in **Figure 3.36**. The data elucidate that complete weight loss incurs between 150 - 180 ^{o}C for both liquids. It is also evident from data that temperature corresponding to maximum weight loss is 169 and 170 ^{o}C for pure DMA and regenerated liquid, respectively. Observed temperatures for maximum weight loss gradient are near to the boiling point of DMA which confirms recycling of spent DMA.

Table 3.3- Wavenumbers corresponding to functional groups identified in FT-IR spectra

S. No.	Band	Wavenumber (cm^{-1})	
1	C-H stretch	3013, 2935	
2	C=O stretch	1747, 1647	
3	C-H bending	1397, 1357	
4	C-N stretch	1265, 1185,1059	[236]
5	C-(CH_3) rocking	1012	[237]

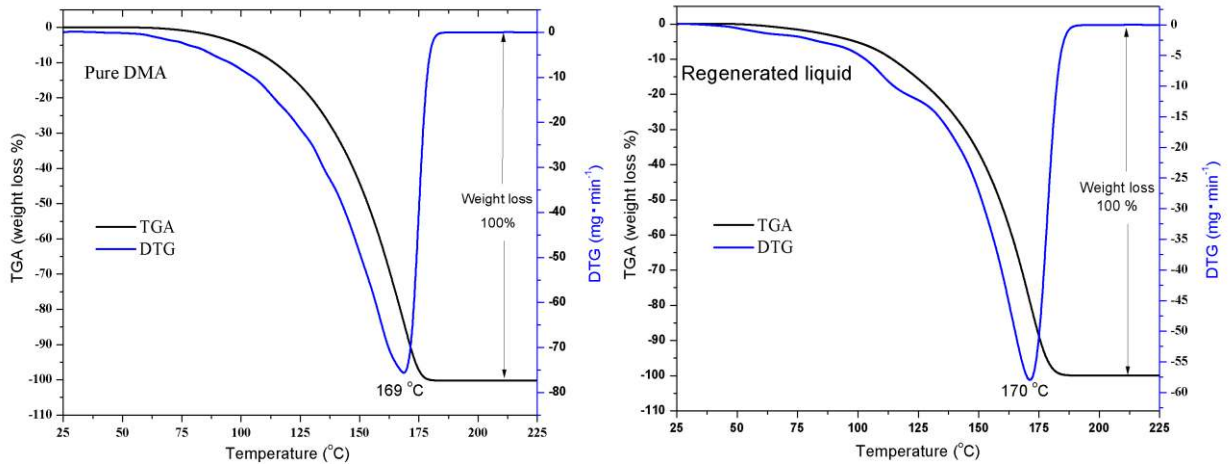

(A) (B)

Figure 3.36- TGA-DTG analysis data of (A) pure DMA and (B) regenerated liquid

The NMR, FT-IR and TGA-DTG analysis validates that regenerated liquid is identical to pure DMA in various aspects. The gas chromatography (GC) is a strong tool to analyze the compound being generated after volatilization or decomposition of liquid product. Therefore, GC of the pure and regenerated liquid has been performed to verify the consistency of previous results. The GC of pure DMA and regenerated liquid showed the presence of similar constituents as the retention time corresponding to peaks

and area under respective peaks were identical (**Figure 3.37**) and thus, corroborates the conclusion drawn by other analysis.

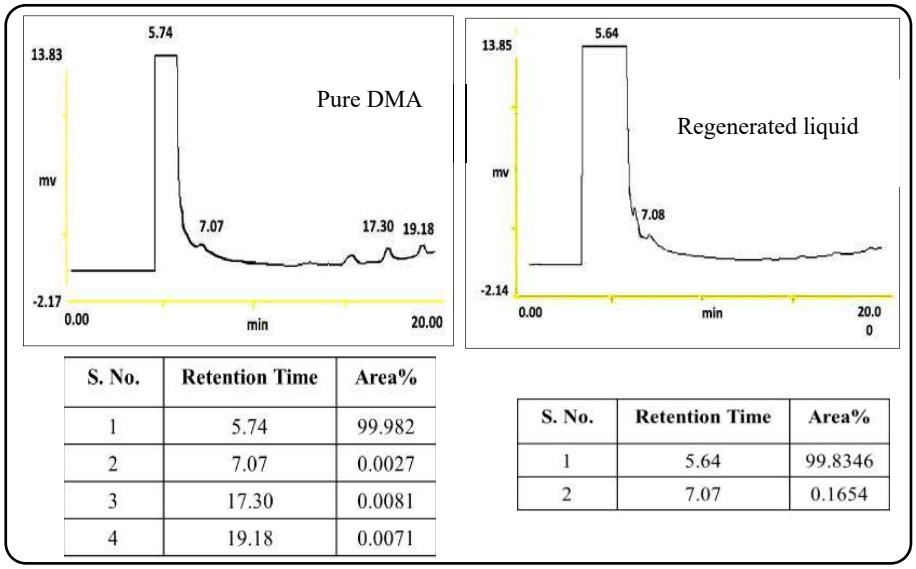

S. No.	Retention Time	Area%
1	5.74	99.982
2	7.07	0.0027
3	17.30	0.0081
4	19.18	0.0071

S. No.	Retention Time	Area%
1	5.64	99.8346
2	7.07	0.1654

Figure 3.37- GC spectrum of pure DMA and regenerated liquid

The identical boiling point, unaltered position of carbon and hydrogen atom, presence of similar functional groups, equivalent thermal degradation profile, and similar species generation after degradation confirms that DMA after usage is entirely recyclable with high purity. This is extremely beneficial towards the cost reduction and environment protection.

3.3.5 HER dissolution efficiency of recycled DMA and its cyclic loss

The efficiency of regenerated DMA to dissolve substrate resin and estimation of the number of cycles associated with the exhaust point has been explored in this work. **Figure 3.38** illustrates the average of the amount of HER dissolved in DMA after 15 cycles of usage and regeneration along with standard deviations. Comparing the HER dissolution data obtained after 15 cycles and pure DMA (after 1st usage), it can be interpreted that after regeneration the HER dissolving capability of DMA is not

affected. It has also been observed that under optimum conditions, 3 – 5 % of poured DMA is not recovered after each cycle. This may be because a small fraction of solvent wetted the glass and WPCBs surface and could not be recovered. After 15 cycles, a significant drop in the HER dissolution has not been found. Thus, it may be assumed that DMA can be recycled infinite cycles although, replenishment of lost solvent after every cycle is essential. Recycling of DMA, negligible drop in dissolution capabilities, and very small loss of solvent after each cycle is very beneficial in view of environmental impact and cost-effectiveness of this proposed process.

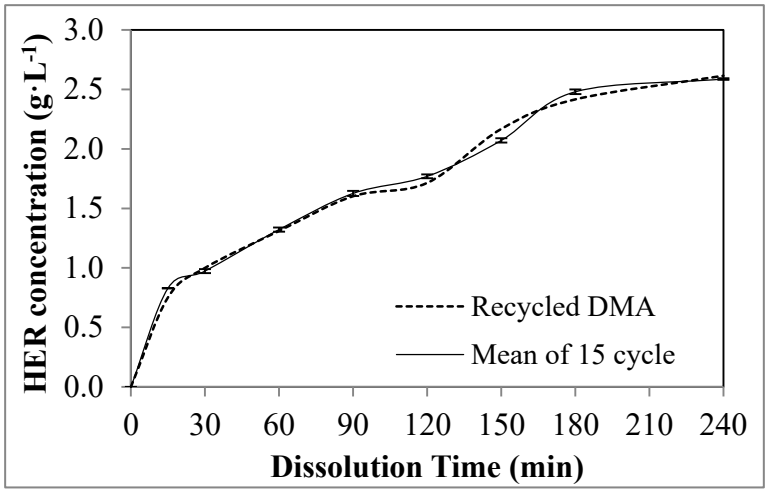

Figure 3.38- Effectiveness of DMA to dissolve HER after15 regeneration cycle

[WPCB:DMA- 3:10, 160 ^{o}C, 4h, WPCB size- 1 cm^{2}]

3.3.6 Analysis of obtained residue after recycling of DMA

The DMA dissolves the substrate resin of WPCBs, and thus, the residue obtained after regeneration of DMA is expected to be the HER. The SEM-EDS, FT-IR, and TGA-DTG analysis of residue has been carried out, and comparative results with untreated HER have been reported. **Figure 3.39** shows the SEM micrograph of untreated HER and residue. It reveals that the particles of untreated HER exerts irregular shape and adhered morphology as it was scratched off from the parent WPCBs. On the other hand,

recovered residue showed the polygon like morphology. The EDS showed the presence of carbon, oxygen, and bromine which are the major constituents of HER polymeric chain. It also revealed that the quantitative composition of untreated HER and residue is nearly equivalent.

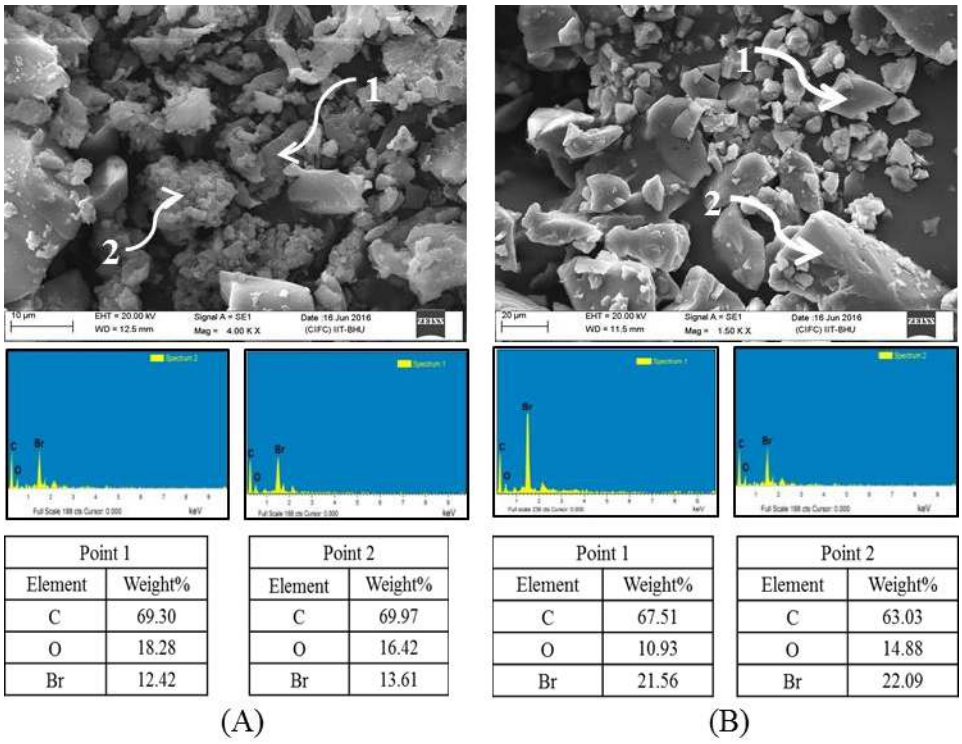

Point 1	
Element	Weight%
C	69.30
O	18.28
Br	12.42

Point 2	
Element	Weight%
C	69.97
O	16.42
Br	13.61

Point 1	
Element	Weight%
C	67.51
O	10.93
Br	21.56

Point 2	
Element	Weight%
C	63.03
O	14.88
Br	22.09

Figure 3.39- SEM-EDX analysis of untreated HER and residue

The FT-IR spectrum of untreated HER and residue is represented in **Figure 3.40**. The FT-IR spectra of both materials have shown vibrations corresponding to para distributed aromatic compound; C-H, C-C, C=C stretching of the aromatic ring. It also showed stretch, bend and rock of alkane; O-H stretch; C-O, C-O-C stretch of ether and stretch of C-Br bonds (please see **Table 3.2.1** for peak indexing). The presence of these bands confirms the co-existence of phenol, ether, aromatic, aliphatic and halogenated hydrocarbons in untreated HER and residue. Thus it can be clinched that residue possess similar structure as the untreated HER.

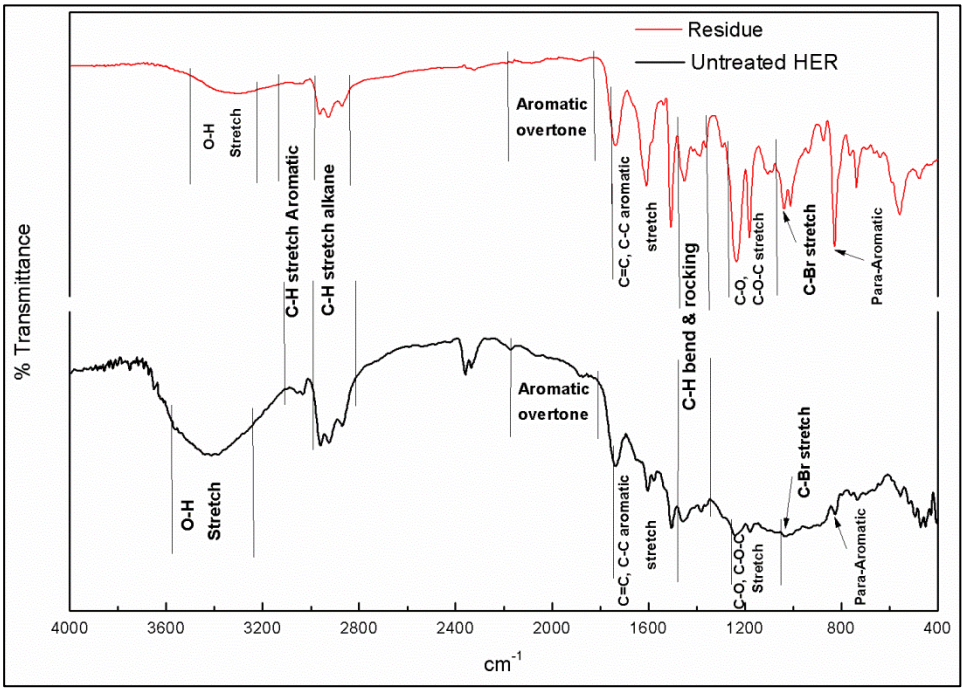

Figure 3.40- FT-IR spectra of untreated HERS and residue

The TGA-DTG of recovered residue and untreated HER have also been carried out to observe the effect of temperature on the degradation of these materials. The results show similar degradation profile having significant weight loss in 280–380 ^{o}C and 290–350 ^{o}C range for untreated and recovered material, respectively (**Figure 3.41**). It also reveals that the maximum instantaneous weight loss occurs at 335 and 330 ^{o}C for untreated HER and residue, respectively. The untreated resin showed 35% weight loss while residue showed 75% loss. This is experienced, because the untreated material was collected by manual scratching of bare WPCBs and thus may contain adhered glass fibre, copper laminates and other material which decomposes at relatively higher temperatures. On the other hand, if the residue is HER than its decomposition will leave back ash and char. The study exposed that weight loss zone and gradient are slightly deviating for both materials. Still, both results are in good agreement with the thermal

degradation data of bare WPCBs discussed in **Section 2.3** and reported in other literature [125,127,134,211].

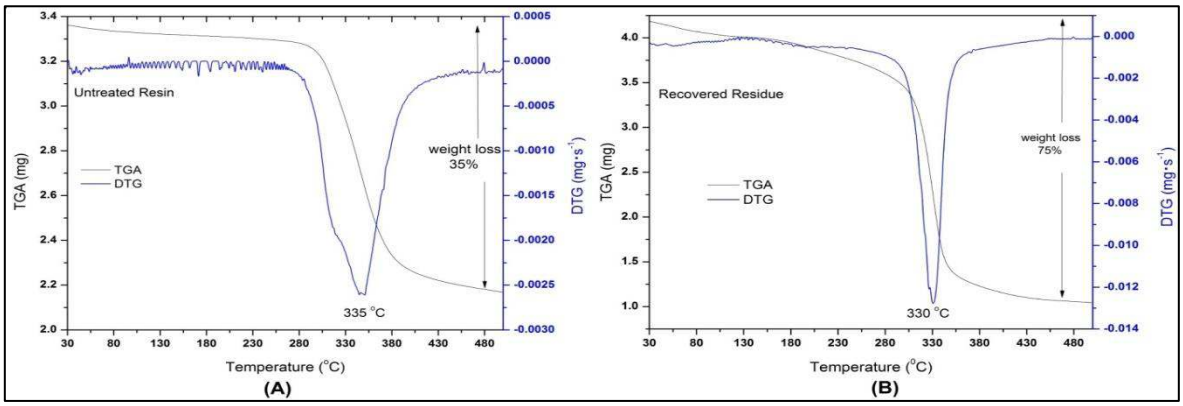

Figure 3.41- TGA-DTG analysis of (A) untreated resin and (B) recovered residue

Identical thermal degradation profile, morphology, composition, and functional groups of untreated HER and recovered residue validates that recovery of dissolved HER during regeneration of solvent.

3.3.7 Possible interaction between HER and DMA

DMA is a dipolar aprotic solvent, having carbonyl and N-C moieties. The carbonyl group exerts high dipole moment due to the presence of oxygen atom and thus acts as a major hydrogen bond acceptor site. The structure of DMA molecule has been shown in **Figure 3.42**. Strong hydrogen bond affinity of DMA and recovery of dissolved solute indicates that hydrogen bond formation between the HER and DMA might be taking place resulting in HER dissolution. The investigation of the exact mechanism of interaction needs significant efforts, yet based on fundamentals of chemistry possible mechanisms are being proposed. The highly electronegative oxygen atom of the carbonyl group of DMA may pull the electron pair of double bond forming a partial single bond. Thus, oxygen atom accepts the hydrogen of the hydroxyl group of parent resin chain, and the bromine of resin pulls the electron towards it leading to the

formation of hydrogen bond (H-O-Br) (**Figure 3.43-A**). The nitrogen atom of DMA and oxygen of resin chain may exert a strong electrostatic force that pulls the electron towards nitrogen atom accepting hydrogen of the hydroxyl group of resin (**Figure 3.43-B**). Methyl group's hydrogen atoms may participate in hydrogen bonding due to the pulling of hydrogen towards electronegative oxygen and bromine atoms of resin chain (**Figure 3.43-**C, D).

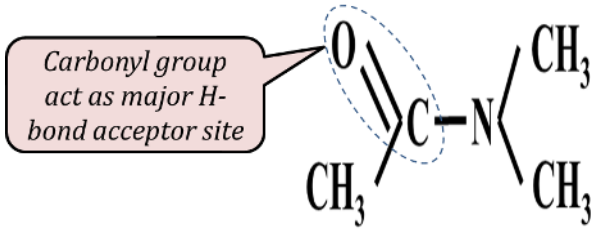

Figure 3.42- Molecular structure of DMA and its major hydrogen bond acceptor moiety

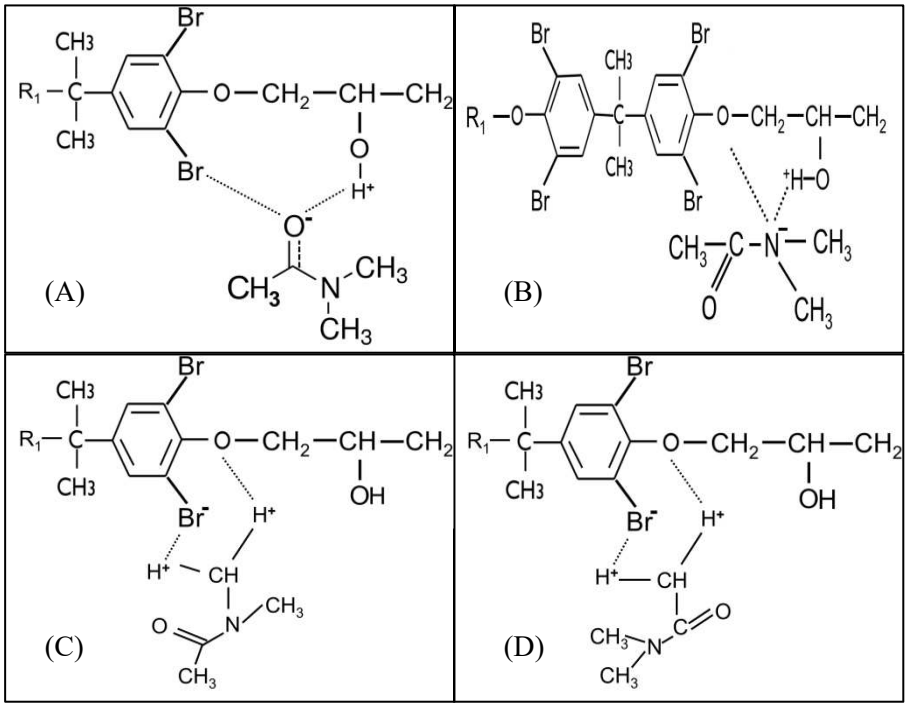

Figure 3.43- Chemical interaction between the substrate resin and DMA resulting dissolution

The present investigation explicated that DMA is a very efficient reagent for HER dissolution similar to DMF. The DMA showed remarkable recyclability and recovery of dissolved HER as it was found in case of DMF. The treatment makes post-hydrometallurgical processing of metallic values easy due to excellent liberation which ensures maximum exposure to lixiviate. This process is an inexpensive alternative to the existing energy-intensive metal-nonmetal liberation and separation process, and at the same time, it ensures cleaner, safer, efficient recycling, and waste management opportunity. The overall flow sheet of the proposed process is shown in **Figure 3.44**.

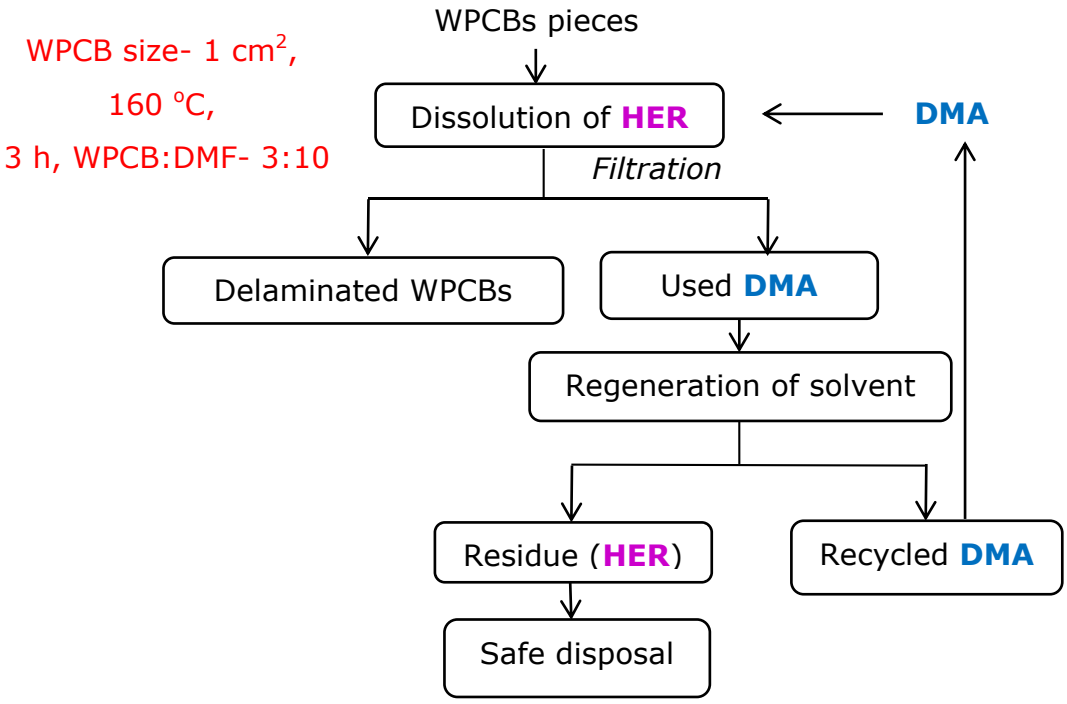

Figure 3.44- Flow sheet of the proposed process for delamination of WPCB using DMA

Conclusions

The investigations demonstrated that solvent DMA is highly effective to dissolve HER of WPCBs. It also dissolved solder mask under an optimized condition which was not evident in case of DMF. The most explicit results observed in the present study are appended below:

- Most efficient dissolution of HER is achieved under conditions *viz.,* WPCB:DMA ratio 3:10, 160 ^{o}C, and WPCB size 1 cm^{2}
- Treatment of WPCBs under these conditions for 3 h results in complete delamination causing liberation of metal laminates.
- Nearly 2.5 g·L^{-1} HER dissolution took place after 3 h reaction under optimized parameters, and progressive dissolution of solder mask is observed.
- It is found that initial quicker reaction zone of DMA with HER at the WPCB's edge is squeezed to 15 min as compared to DMF (~30 min)
- Above two factors gives a clue that probably DMA is more aggressively reacting with HER still it needs further investigations.
- The efficient recyclability of spent solvent, recovery of dissolved residue, and negligible HER dissolution capacity are the other results found during the present study. These results are quite similar to the results found in case of DMF.
- The studies showed that hydrogen bonding might be responsible for the dissolution of HER in the solvent.

Section- 4

Comparative study of HER dissolution in DMA vs. DMF and its mechanism

3.4 Comparative study of HER dissolution in DMA *vs.* DMF and its mechanism

3.4.1 Dissolution of HER in DMA *vs*. DMF

The study of HER dissolution in solvent DMA and DMF showed a similar effect of temperature, WPCB:solvent ratio, and WPCB size. Although, the optimized conditions are: 160 ^{o}C, 3 h and 135 ^{o}C, 4 h, respectively for DMA and DMF but both resulted in 2.5 g•L^{-1} HER dissolution at WPCB:solvent ratio of 3:10. Investigations also exposed that DMA dissolves the solder mask layer and acquires a squeezed initial HER dissolution zone. So it may be predicted that DMA might be a more effective solvent for resin dissolution. Hence, to understand the relative goodness of solvent(s), a comparative study has been carried out under identical experimental conditions and results are discussed below:

3.4.1.1 HER dissolution in DMA vs. DMF at varying temperature

To examine the relative effectiveness of solvent, HER dissolution at 120 ^{o}C and 140 ^{o}C has been carried out. The investigated temperatures are chosen in a way that role of rupture of *Van der Walls'* bond on the effectiveness of dissolution can also be monitored. Thus, the lower temperature is set 10 ^{o}C below T_g and higher was set 10 ^{o}C above T_g. Other parameters chosen were: WPCB:solvent- 3:10, 4 h, and WPCBs size- 2.25 cm^2. The HER dissolved at both temperatures at a different time in DMA and DMF are shown in **Figure 3.45**. Results showed that after 1 h, DMA dissolved 75 % more resin than DMF irrespective of temperature. At 120 ^{o}C, HER dissolution in DMF after 4 h reached to 0.9 g·L^{-1} from 0.33 g·L^{-1} which incurred after 15 min. On the other hand, the DMA dissolved 0.69 g·L^{-1} HER after 15 min which further rose to 1.59 g·L^{-1} after 4 h. Further, within 4 h at 140 ^{o}C, nearly 1.15 g·L^{-1} and 2.02 g·L^{-1} of HER got dissolved

in DMF and DMA, respectively. The rise in temperature led to 30% more HER dissolution in DMA. The nature of curve also elucidates that more HER solvation in DMA is taking place at higher temperatures, relatively. At 120 ^{o}C, the curve possesses a slope (m) of 5.099 and 3.011 for DMA and DMF, respectively (**Figure 3.45**). Later it increased to 6.67 and 3.43 at 140 ^{o}C for DMA and DMF, respectively. Further at a higher temperature, the increase in slope of the curve is more for DMA than DMF. This explains that DMA exhibits pronounced effect of the rise in temperature i.e. quicker dissolution rates. It points out that higher temperature than T_g ensures more dissolution as the breakage of *Van der Walls'* bond triggers dissolution. Another major reason for better dissolution in DMA is its higher dipole moment (3.79×10^{-29} C·m at 20 ^{o}C) and dielectric constant (37.8 at 10 kHz) compared to DMF (please see **Table 2.1**). Since HER is a polar substance and polar material are prone to dissolution in a solvent having a stronger dipole moment and dielectric constant.

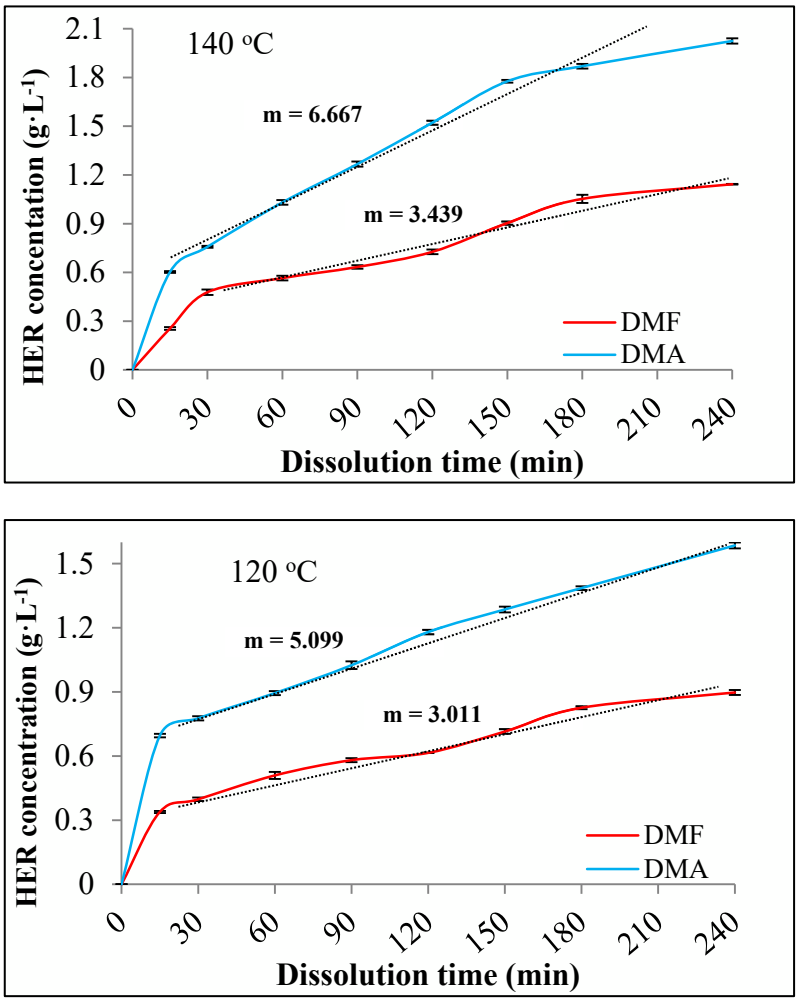

Figure 3.45- Effect of temperature on the dissolution of HER

[WPCBs: solvent– 3:10, 2.25 cm^2]

3.4.1.2 Effect of WPCB:solvent ratio on relative dissolution of HER

Investigation of HER dissolution in both solvent under varying WPCB:solvent ratio has been studied and shown in Figure 3.46. The increase of WPCBs:solvent ratio registered more resin dissolution due to higher utilization of solvents. The 3:10 is the limiting ratio as the higher ratio is associated with incomplete contact of WPCB with solvent and excessive swelling as discussed in **Section 3.2.2**. Data shows that after 4 h reaction, DMF dissolved 0.62, 1.01 and 1.14 $g \cdot L^{-1}$ HER at WPCB:DMF of 1:10, 2:10 and 3:10, respectively. On the other hand, DMA dissolved 0.93, 1.54 and 2.02 $g \cdot L^{-1}$ of HER at

same ratios (**Figure 3.46**). Thus, it can be deduced that DMA is 50-77% more efficient than DMF at varying WPCB:solvent ratios. Further, the HER dissolution efficiency of DMA rose by 217% as WPCB:DMA increased to 3:10 from 1:10. It may be because, DMA possesses higher molar volume (93 $mL \cdot mol^{-1}$) than DMF (please see **Table 2.1**) and thus, ensures more reagent availability, better penetration of solvent in WPCBs, and faster reaction rates. Noteworthy, the WPCBs of 2.25 cm^2 were completely separated into glass fibre matrix, copper layers after 180 min under conditions *viz.,* WPCBs: solvent – 3:10 and 140 ^oC.

3.4.1.3 Influence of WPCB size on resin dissolution in solvents

Influence of WPCBs size on the relative dissolution of HER in DMA and DMF has been probed by varying size (2.25 cm^2, 6.25 cm^2, 12.25 cm^2 and 20.25 cm^2) under WPCB:solvent ratio of 3:10 and 140 ^oC. Data shows that DMA is relatively better for all size feed material although the resin take-up drops with an increase in size (**Figure 3.47**). This is because of the lower number of *'through hole'* and minimal face to face sticking of WPCBs pieces together. The observation also revealed that HER dissolution efficiency of DMF is more affected by an increase in WPCBs size. For example, the HER dissolution rise of minimal 260% after 4 h compared to level after 30 min for DMA for all feed size. Further, during the same interval using DMF, an increase of 237%, 63%, 31% and 17% has been experienced for size 2.25 cm^2, 6.25 cm^2, 12.25 cm^2 and 20.25 cm^2, respectively.

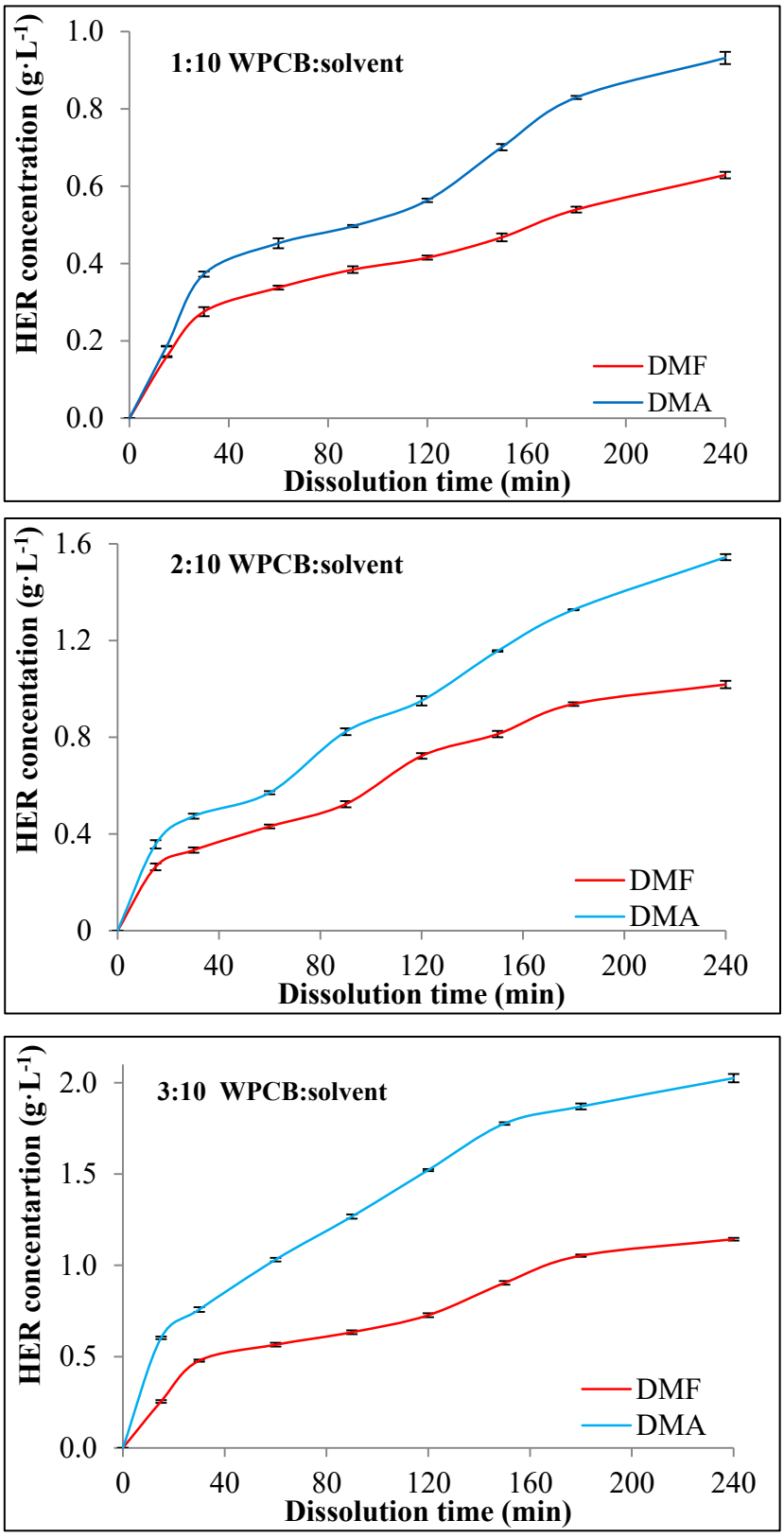

Figure 3.46- Effect of WPCB:solvent on the dissolution of HER

[140 ^{o}C, 4 h WPCBs size- 2.25 cm^{2}]

The data interpretation also showed maximum dissolution efficiency for WPCBs of 2.25 cm^2 in DMA. For WPCBs of 6.25 cm^2, 12.25 cm^2 and 20.25 cm^2, DMA showed 83%, 94%, 122% higher resin dissolution than DMF (**Figure 3.47**). Since, DMA possesses higher heat capacity (178 $J \cdot K^{-1} \cdot mol^{-1}$) than the DMF (120 $J \cdot K^{-1} \cdot mol^{-1}$), thus higher heat flux is available surrounding the WPCBs. It may be the reason behind better resin dissolution in DMA than DMF.

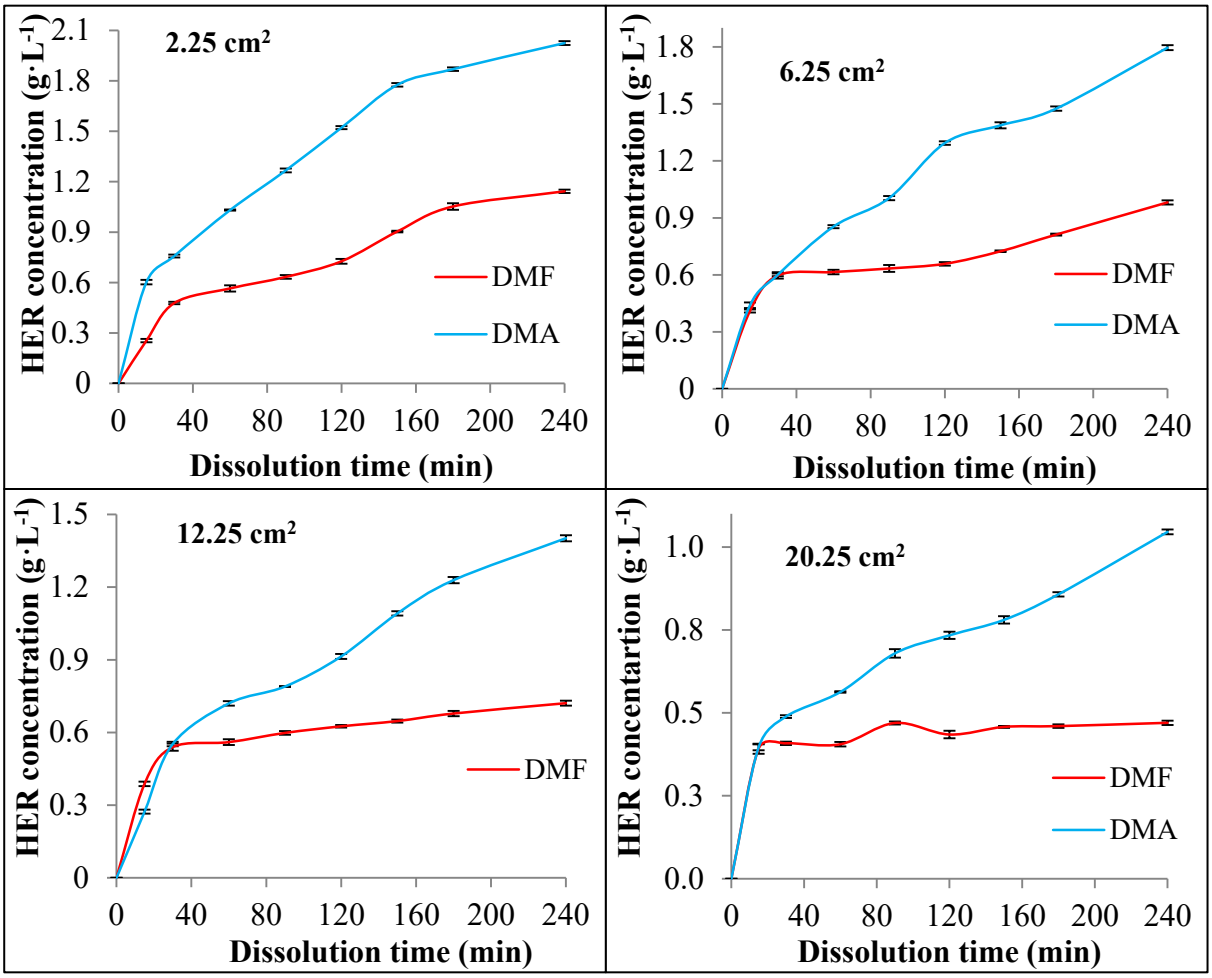

Figure 3.47- Effect of WPCBs size on dissolution of HER

[WPCB:Solvent- 3:10, 140 ^oC, 4 h]

Based on the above studies it has been found that DMA is a better solvent for substrate resin dissolution, subsequent delamination, and separation of WPCBs layers. Yet, exact mechanism responsible for dissolution needs further investigations.

3.4.2 Mechanism of dissolution of HER in DMA

The previous studies showed that solvent DMA is more efficient for the dissolution of HER. The investigation and hypothesis expressed some putative interpretation about the mechanism of solvent interaction with PCBs, but exact mechanism was not explored. Therefore, a thorough investigation has been carried out to expose the nature of the interaction of resin substrate with DMA and reported as given below.

3.4.2.1 Identification of HER dissolved in solvent

To understand the mechanism of interaction, WPCBs has been treated by using DMA under optimized conditions *viz.,* WPCB:DMA- 3:10, 160 ^{o}C, 1 cm^2 for 8 h. The NMR analysis of the spent DMA samples after 8 h has been carried out to identify the subsequent changes in chemical structure of DMA due to dissolution. The proton NMR spectrum of DMA after 8 h contact with WPCBs is shown in **Figure 3.48**. The proton linked to the aromatic chain showed a signal at 7.11 ppm. At 4.209 and 3.683 ppm, signals for the proton of the ether linkage of HER chain are found. The proton of hydroxyl moiety showed a signal at 1.321 ppm while protons of methyl group surrounded by aromatic molecule showed a signal at 1.611 ppm. The peak values of respective proton of different positions are shown in **Table 3.4**. The signals corresponding to DMA have also been observed at 3.03, 2.93 and 2.07 ppm (similar to results reported in **Section 3.3.4)**.

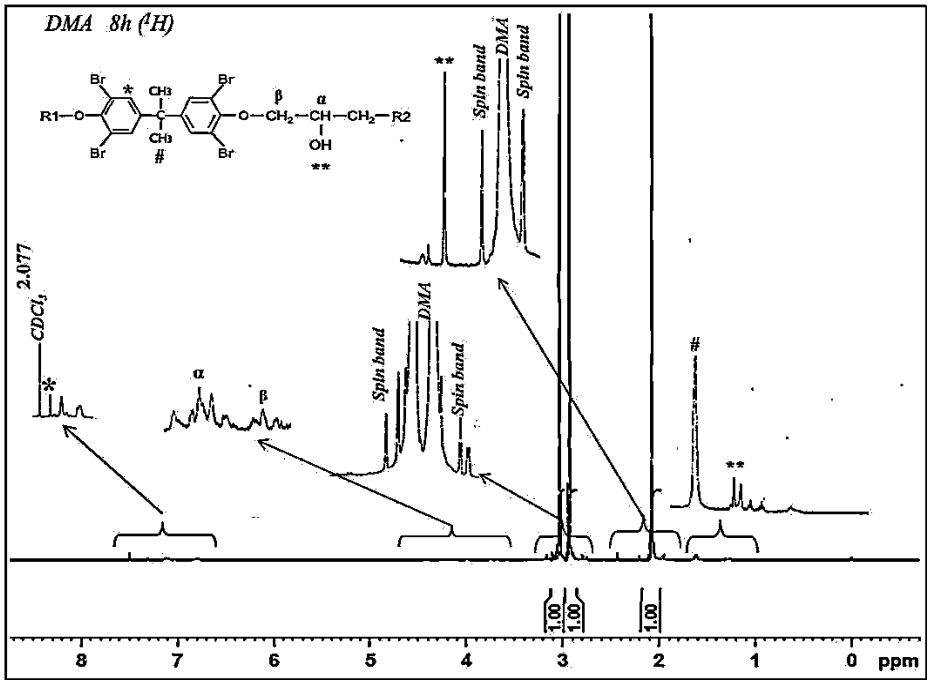

Figure 3.48- ^{1}H-NMR of DMA containing HER after 8 h

Table 3.4- NMR signals of proton at different position in HER chain (as indexed in **Figure 3.48**) (Please see Appendix A for peak identification)

Position of H atom	**Signal (ppm)**
Linked to aromatic (*)	7.11
Position #	1.611
Position β	3.683
Position α	4.209
Position **	1.321

The **Figure 3.49** shows the carbon NMR spectrum of pregnant DMA after 8 h reaction. Spectrum analysis revealed that peaks corresponding to the parent carbon atom of HER are present along with the peaks of DMA. The carbon of aromatic chain adjacent to ether link and opposite side showed a signal at 162.5 and 68.9 ppm, respectively. Carbon atom at bromine substituted moiety showed a signal at 110.5 ppm.

Further, the carbon atom of the aromatic chain having no substitution showed a signal at 129.1 ppm. The methyl moiety and the carbon atoms connecting both aromatic chains registered their existence at 25.8 and 68.9 ppm, respectively. The carbon of ether branch associated with hydroxyl moiety showed a signal at 66.5 ppm. The rest two carbon atoms of ether branch showed their presence at 30.1 ppm. The carbon of DMA molecules also showed signals at 170.225, 37.683, 34.725, and 21.177 ppm (similar to results reported in **Section 3.3.4**). The signals corresponding to respective carbon atoms (indexed as a, b, c,….g) in the spectrum are shown in **Table 3.5**. The NMR analysis showed that the dissolved HER in the DMA may be easily identified. The analysis also showed that the whole HER chain is distinguishable in NMR spectra along with the unaltered positions of DMA. It strengthens the prediction that HER dissolution is a solvation reaction rather than molecular exchange reaction.

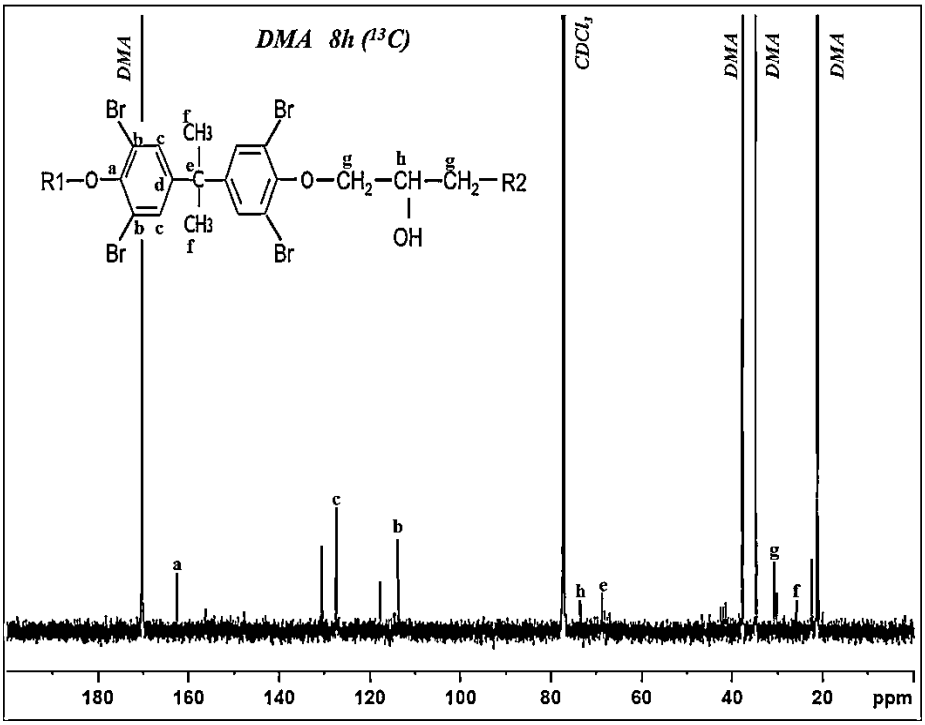

Figure 3.49- ^{13}C-NMR of DMA containing HER after 8 h

Table 3.5 - NMR signals of carbon at different position in HER chain (as indexed in **Figure 3.49**) (Please see Appendix A for peak identification)

Position of C atom	Signal (ppm)
Position a	162.5
Position b	110.5
Position c	129.1
Position d	147.3
Position e	68.9
Position f	25.8
Position g	30.1
Position h	66.5

3.4.2.2 Identification of nature of interaction of HER with DMA

The proton-NMR of DMA loaded with HER after different time (1, 2, 3, 4 and 8 h) has been carried out to identify any change in the respective positions of protons. The spectra of representative samples drawn after different time intervals are shown in **Figure 3.50**. It is evident from the NMR spectrum that peaks corresponding to hydrogen atoms of HER chain appeared just after 1 h of reaction. Further, these peaks kept intensifying as the reaction proceeds for a longer time. This also indicates that amount of HER dissolved in DMA keeps on rising w.r.t. contact time. The comparative evaluation of spectra revealed that proton peak of hydroxyl (O-H) group of HER is changing its position w.r.t. time. The signal of proton of O-H group is evident at 1.263 ppm after 1 h of reaction. Later, it shifted to 1.267 and 1.312 ppm after 2 h and 8 h, respectively (indicated with red arrows in **Figure 3.50**). Thus, it is clear that the proton

peak of hydroxyl moiety is shifting to higher frequency with time. The hydroxyl group acts as a hydrogen donor moiety, and shift of proton donor peak towards higher frequency is common in hydrogen bonding [230]. The phenomenon of shifting is seen due to the reduced density of electron cloud surrounding the proton H-bonding takes place. Therefore, above investigations confirm the involvement of O-H moiety of HER chain in hydrogen bonding.

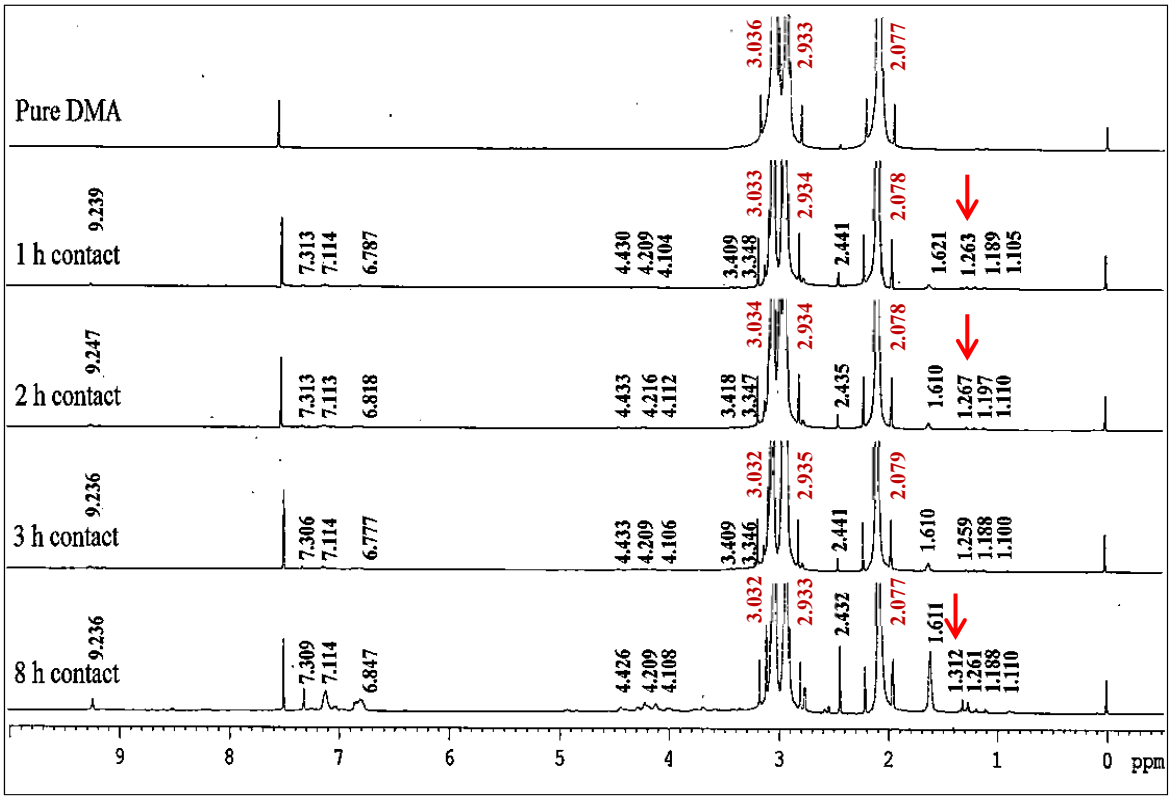

Figure 3.50- ^{1}H-NMR spectra of pregnant DMA after different time interval

It is also evident that the peaks of DMA molecule are not shifting their respective positions with time. Thus, the hypothesis of participation of methyl moieties of DMA molecule in hydrogen bonding (**Figure 3.43- C,D**) is laid off. Yet, it is still a dilemma that whether the carbonyl or amide moiety is participating in hydrogen bonding with hydroxyl of HER. Thus studies have been extended to FT-IR analysis of representative

samples. The FT-IR spectrum of pure DMA and representative samples are shown in **Figure 3.51**. It reveals the existence of the peak corresponding to para-distributed aromatic (833-835 cm^{-1}); C-H stretching (2935 cm^{-1}), bending, and rocking; C-C and C=C ring stretching (1680-1510 cm^{-1}); C-Br stretch (1028 - 1009 cm^{-1}) etc. after 1 h. Later, the intensity of peak kept rising as time elapsed specifying more resin take-up in DMA. The respective peaks of carbonyl (1641 cm^{-1}) and C-N (1059-1265 cm^{-1}) of DMA have also been found to co-exist in the FT-IR spectra after 1 h. The spectral analysis exposed the shifting of carbonyl and hydroxyl peaks to lower web numbers with increased reaction time. The carbonyl peak originally at 1647 cm^{-1} shifted to wavenumbers 1641, 1638, 1635 and 1634 cm^{-1} after 1 h, 2 h, 3 h and 8 h reaction, respectively. The broadening of carbonyl peak with increase in reaction time is also evident. Contrary, hydroxyl peak shifted to lower frequency *viz.,* 3493, 3479, 3463 cm^{-1} after 1 h, 3 h and 8 h, respectively from the original position of 3568 cm^{-1}.

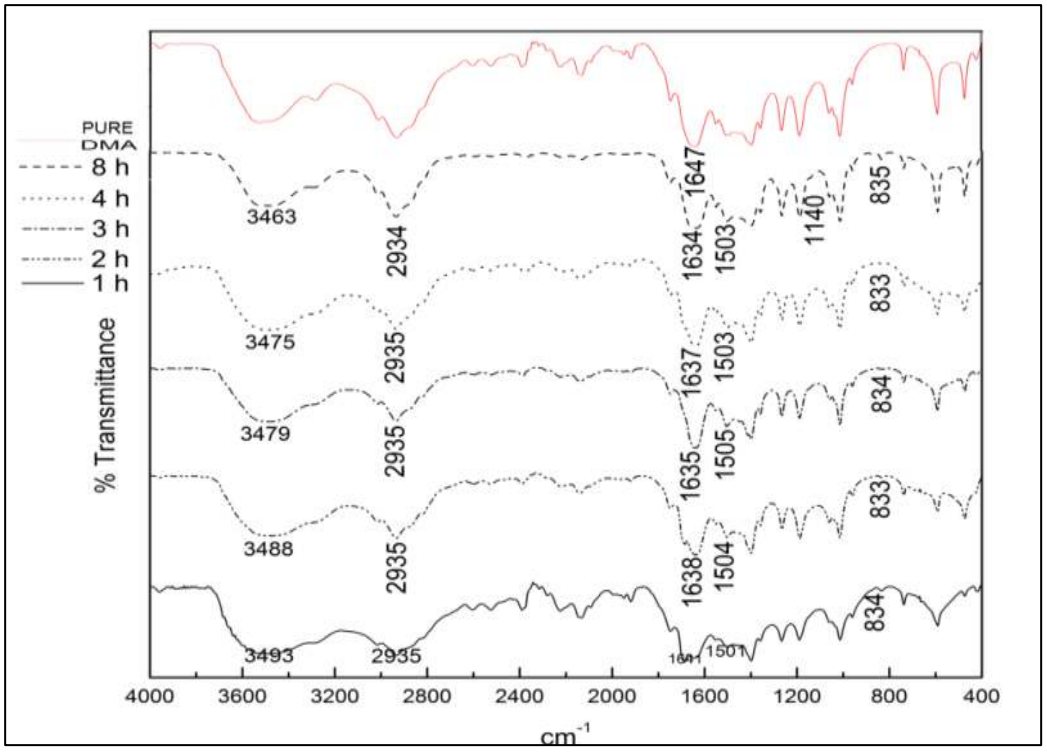

Figure 3.51- FT-IR of HER dissolved in DMA after varying DMA-PCB contact time

The carbonyl is a proton acceptor moiety present in DMA while O-H is a proton donor moiety present in HER. The shifting of the proton donor and acceptor group towards the lower frequency is a consequence of hydrogen bond formation [230]. These studies confirm that HER dissolution in DMA is due to the formation of hydrogen bond between carbonyl and hydroxyl group of DMA and HER, respectively. Once the H-bonding takes place, the shift of proton donor is more dominant than acceptor group and the same has been registered in the present system. The carbonyl and hydroxyl group shifted to lower frequency by 13 cm^{-1} and 105 cm^{-1}, respectively. This further corroborates with the previous results. The study fortifies the hypothesis of HER dissolution as a cause of hydrogen bond formation. The chemical reaction responsible for the dissolution of resin has also been represented in **Figure 3.52.**

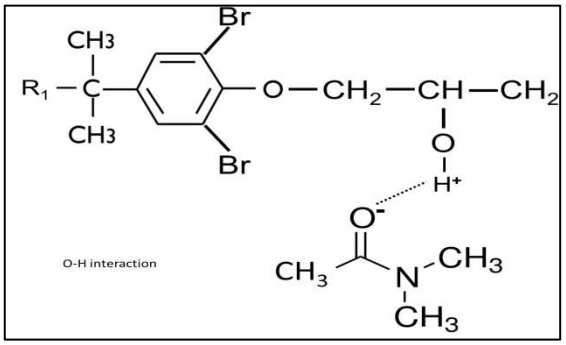

Figure 3.52- Chemical reaction taking place during DMA-PCB interaction

Conclusions

The comparative study showed the excellent dissolution of HER in solvent DMA than DMF. Exploration of the mechanism of reaction between HER and DMA revealed the important role of hydrogen bonding. The major conclusions are given as follows:

- DMA dissolves 77 % more resin than DMF under conditions *viz.,* WPCB:solvent- 3:10, 140 ^{o}C, 4 h and WPCB size- 2.25 cm^{2}
- Resin dissolution in the solvents varies inversely with the size of WPCBs. Its dissolution in DMF falls rapidly as the size increases and the rate of dissolution is less in DMF compared to DMA for larger size WPCBs.
- The effectiveness of removal of resin from parent WPCBs increases with an increase in temperature and WPCB:solvent ratio. Solvent DMA registered 30% more resin dissolution at 140 ^{o}C than 120 ^{o}C.
- The study of mechanism showed that the carbonyl moiety of DMA forms a hydrogen bond with the hydroxyl group of HER.
- The phenomenon of hydrogen bonding is responsible for the dissolution of HER in DMA.

Section- 5

Delamination of large size WPCBs and post-treatment leaching of copper

3.5 Delamination of large size WPCBs and post-treatment leaching of copper

3.5.1 Utility of DMA for delamination of large size WPCBs

The previous studies showed that DMA is more efficient solvent for dissolution of HER and its separation from parent WPCBs. The study also showed the best delamination for 1 cm^2 size within 3 h under WPCB:DMA ratio of 3:10. The mechanism study also revealed that H-bonding is a precursor of dissolution. Observation of the progressive dissolution of HER indicates that relatively slower delamination takes place for larger size WPCBs. It is anticipated that probably more reaction time is required for complete delamination of larger WPCBs. Thus, investigations have been extended to study the delamination of WPCBs of 4, 9 and 16 cm^2 size under varying temperatures and time. The investigation regarding delamination of larger size WPCBs is required to overcome the difficulty of cutting down of WPCBs to a smaller size which requires higher energy consumption in doing so.

3.5.1.1 Delamination of WPCBs of 4 cm^2

The WPCBs of 4 cm^2 size have been treated by DMA at 120, 140 and 160 ^oC for 4 h at 3:10 WPCB:DMA ratio. As discussed in **Section 3.3.1**, better delamination is experienced at a higher temperature. It is found that, at 120 ^oC, rate of delamination is quite slow. Neither, solder mask dissolution (after 3 h) nor significant delamination has been observed after 4 h (**Figure 3.53-B,C**). As the temperature rose, better delamination and improved dissolution of solder mask have been acquired. After 3 h, at 160 ^oC satisfactory delamination has been achieved with the considerable dissolution of 'Solder mask'.

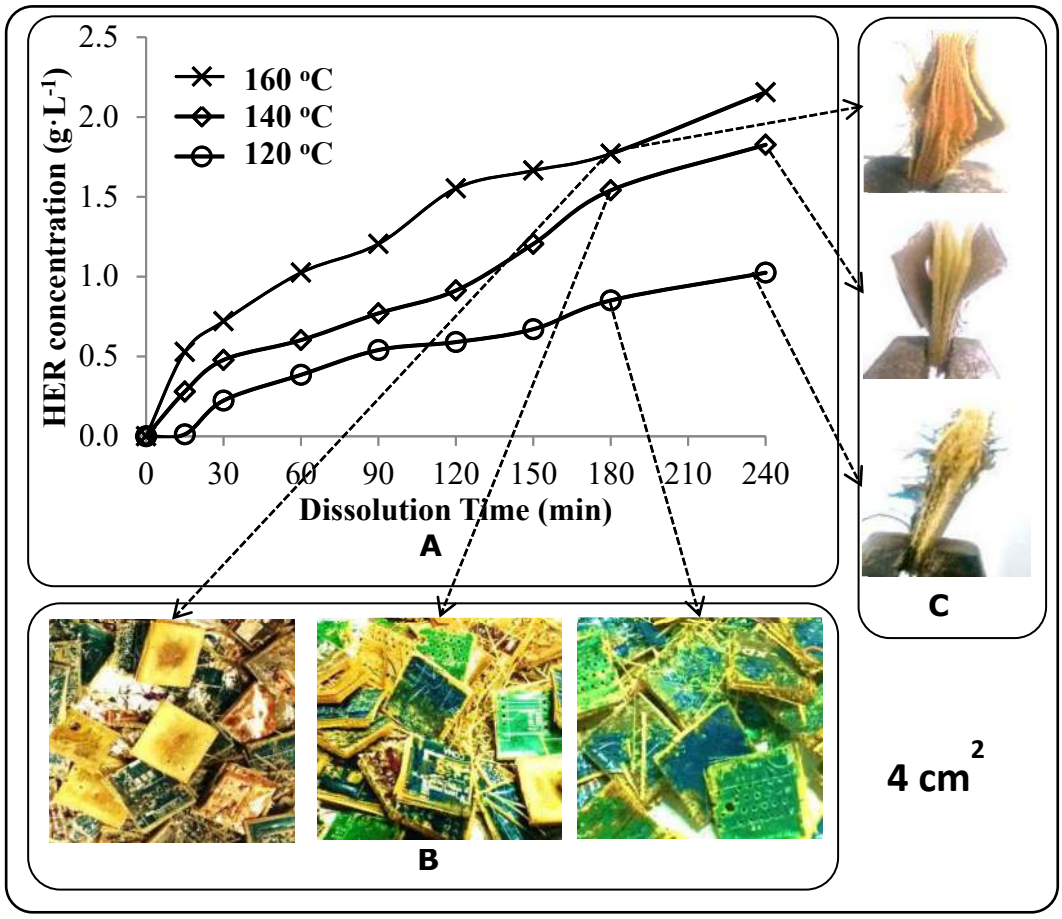

Figure 3.53- (A) Effect of temperature on HER dissolution, (B) Treated PCBs after 3 h, (C) Cross-section of treated PCBs [WPCB:DMA- 3:10, 4 h, WPCB size- 4 cm^2]

3.5.1.2 Delamination of WPCBs of 9 cm^2 size

The WPCBs of 4 cm^2 size were delaminated after 3 h and the larger size is expected to consume more time for delamination. Thus, for 9 cm^2 size, experiment duration has been extended to 8 h. The HER dissolution data at different temperature and treated WPCBs after various time are shown in **Figure 3.54**. It is found that after 5 h, evidence of solder mask dissolution has been noticed at 160 ^oC (**Figure 3.54-B**). Further, substantial delamination is evident after the prolonged reaction. At 120 ^oC, WPCB of 9 cm^2 exerted initial delamination from the edge which after 8 h and it further improved with rise in temperature (**Figure 3.54-C**). At 160 ^oC, significant delamination of the fed

WPCBs has been seen after 5 h. The study shows that with increase in the size of WPCBs, difficulty in the delamination is being experienced.

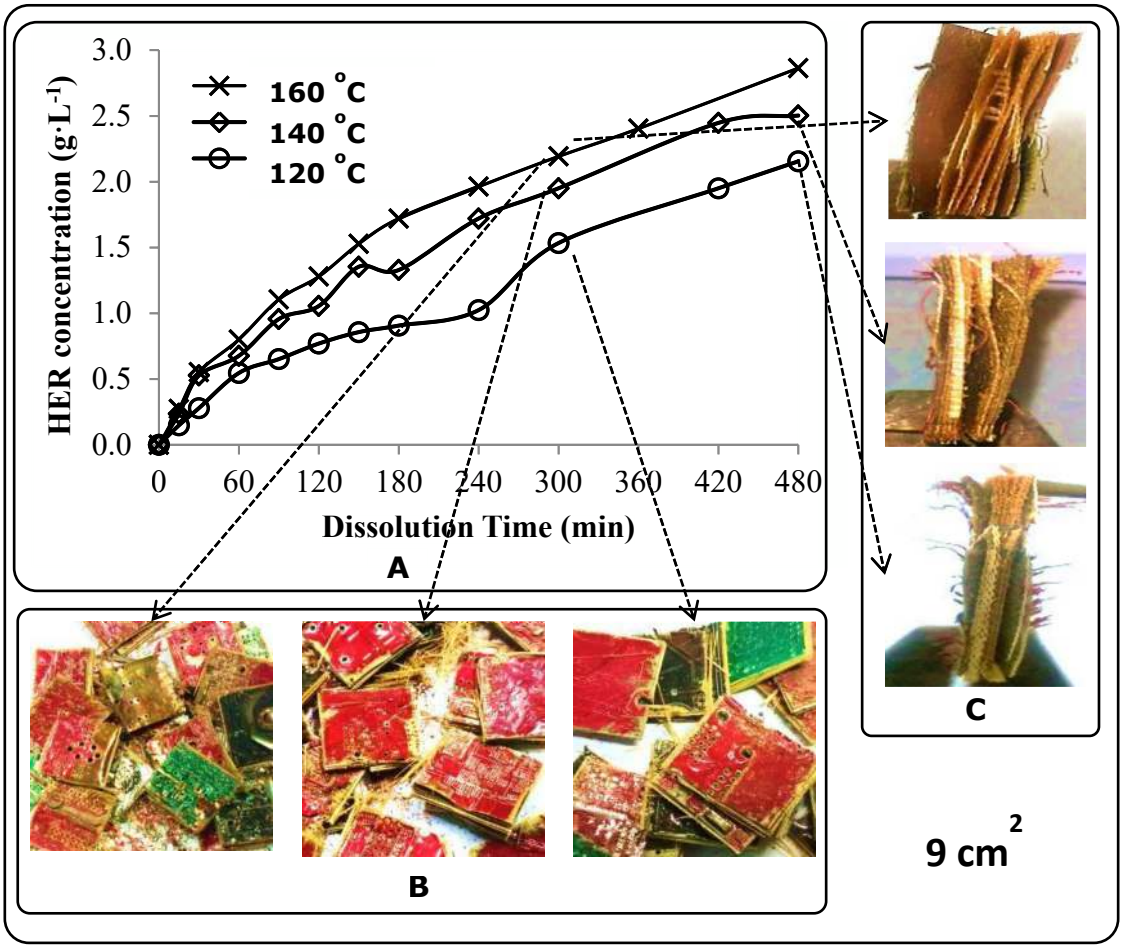

Figure 3.54- (A) Effect of temperature on HER dissolution, (B) Treated WPCBs after 5 h, (C) Cross-section of treated PCBs [WPCB:DMA- 3:10, 4 h, WPCB size- 9 cm^2]

3.5.1.3 Delamination of WPCBs of 16 cm^2 size

Keeping the previous results in mind, the 16 cm^2 size WPCBs has been subjected to 9 h of treatment. The similar results have been registered as found in case of 9 cm^2 size. At low temperature, the only delamination near the edge of WPCBs has been seen after 9 h, while no evidence of 'Solder mask' dissolution was observed (**Figure 3.55**). As the temperature rose to 140 ^oC, partial dissolution of solder mask is seen after 7 h time.

Further, significant delamination has been seen after 7 h at 160 °C but complete delamination couldn't be achieved even after 9 h.

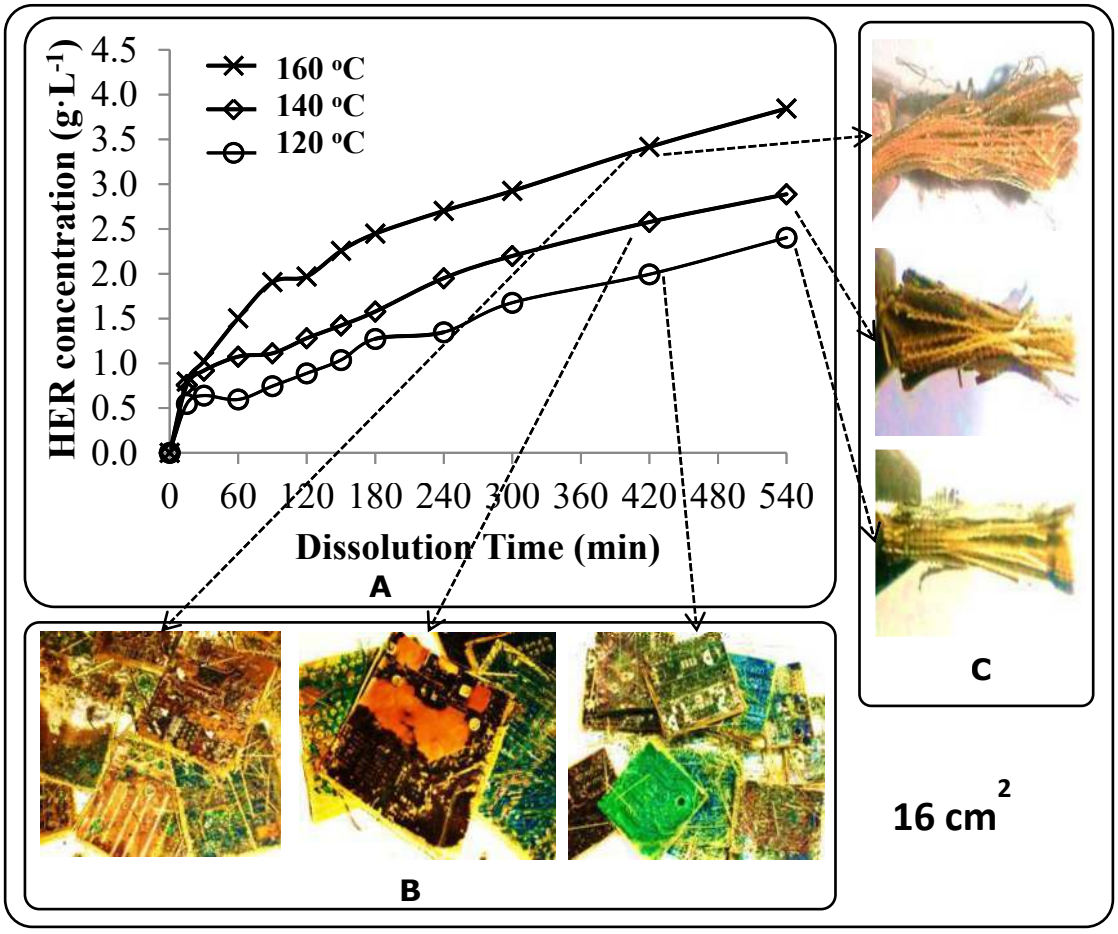

Figure 3.55- (A) Effect of temperature on HER dissolution, (B) Treated PCBs after 7 h, (C) Cross-section of treated PCBs [WPCB:DMA- 3:10, 4 h]

The nature of curve shows that the dissolution is continuously increasing yet, experimental time was limited to 9 h because the prolonged reaction requires more energy and an experiment for extended duration may consume more energy than required for the chopping WPCBs to a smaller size. Considering these factors, it is experienced that for the better economy the WPCBs may be downsized to smaller sizes.

3.5.2 Effect of organic solvent treatment on leachability of copper

The present research work has been carried out to explore a new WPCB's pre-processing technique that may ensure cost-effective liberation of metal values. The investigated technique of dissolution and separation of HER from parent WPCBs by using DMA resulted in the exposure of the metallic surface of WPCBS. The treatment of these metallic surfaces by leaching agents may result in better recovery of copper and other valuable metals. The studies also revealed that, after DMA treatment under optimized conditions, the copper laminates with nearly 20% of nonmetallic fraction were still left in WPCBs (**Section 3.3.3)**. On the other hand, the hammer milling resulted in the improvement of grade of Cu from 22% to 43% with 87% recovery (**Section 3.1.4)**. Thus, in order to investigate the effect of DMA treatment on leachability of copper the comparative leaching studies have been performed. The copper has been leached under conditions *viz.*, 140 ^{o}C, 3M H_2SO_4 and pulp density 50 $g \cdot L^{-1}$ (reported by Basha, (2017)) under varying time and concentrations of oxidants hydrogen peroxide (H_2O_2) and nitric acid (HNO_3). The **Figure 3.56** shows the effect of variation of H_2O_2 on the leaching of copper. It is evident that high concentration of oxidant in sulphuric acid improves the dissolution of copper significantly. Data shows that using 5% H_2O_2 only 62.5% copper has been leached out after 75 min and leaching rose to 93.5% at 15% H_2O_2. The nature of curve also reveals that the dissolution of copper takes place gradually with time in presence of H_2O_2. On the other hand, copper leaching under varying nitric acid concentrations showed that a small concentration is sufficient to leach a significant amount of copper (**Figure 3.57**). The curve also elucidates that the leaching of copper is quite fast in HNO_3 compared to H_2O_2. In 15 min time, ~ 45% copper dissolution has been registered by using 5% HNO_3 while 5%

H_2O_2 resulted in 18% copper dissolution. Further, a considerable fraction of copper is dissolved in 3M sulphuric acid in presence of HNO_3 within 30 min time and later the dissolution rate is relatively slower. e.g., at 30 min, ~76% copper dissolution took place using 5% HNO_3 and it further rose to 95% after 75 min.

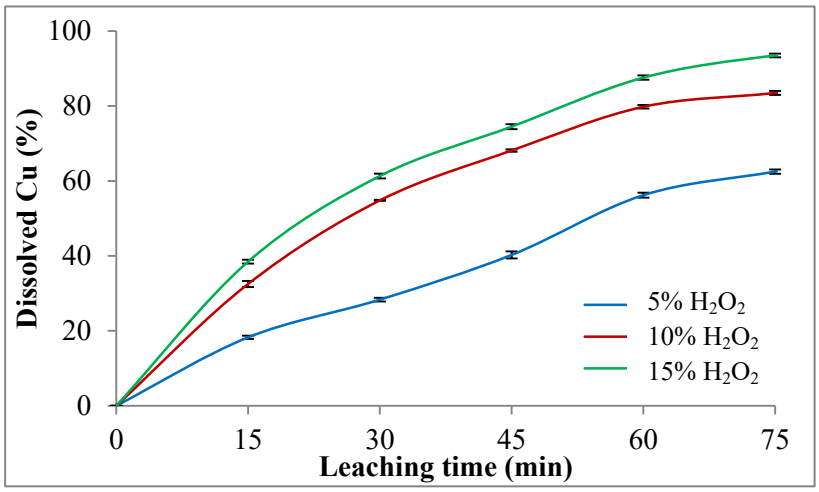

Figure 3.56- Leaching of Cu from copper laminate of DMA treated WPCBs under varying concentration of oxidant hydrogen peroxide

[3M H_2SO_4, 140 °C, WPCBs size- 2.25 cm^2, pulp density 50 $g \cdot L^{-1}$]

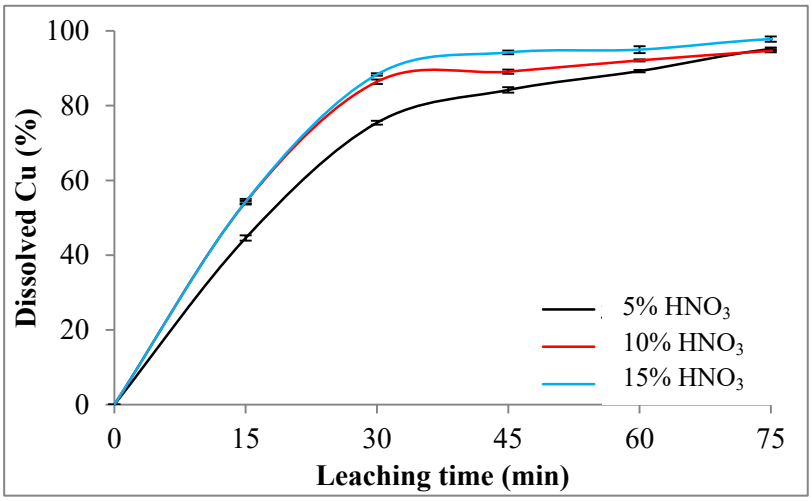

Figure 3.57- Leaching of Cu from copper laminate of DMA treated WPCBs under varying concentration of oxidant nitric acid

[3M H_2SO_4, 140 °C, WPCBs size- 2.25 cm^2, pulp density 50 $g \cdot L^{-1}$]

Above studies indicated that copper can be easily dissolved by using nitric acid as compared to hydrogen peroxide. Under similar conditions, 96% copper has been leached out by using 5% HNO_3 while using 15% H_2O_2 nearly 93% copper has been leached out. The leachability of copper has also been investigated from the WPCBs having enriched copper content (43 wt%) which has been obtained by after hammer milling and sieve analysis (please see **Section 3.1.4** for details). The **Figure 3.58** shows that by using 5% HNO_3 as oxidant only 50% copper could be leached. Increase in concentration of HNO_3 to 15% resulted in 94% copper recovery. On the other hand, 15% hydrogen peroxide resulted in only 43% copper recovery.

The comparative studies of leaching of copper show that 96% Cu can be leached out from DMA treated WPCBs by using 5% nitric acid while 15% HNO_3 is required to leach ~ 94% copper from hammer milled WPCBs. Further, by using 15% hydrogen peroxide, 94 % and 43% copper has been leached from DMA and hammer mill treated WPCBs, respectively.

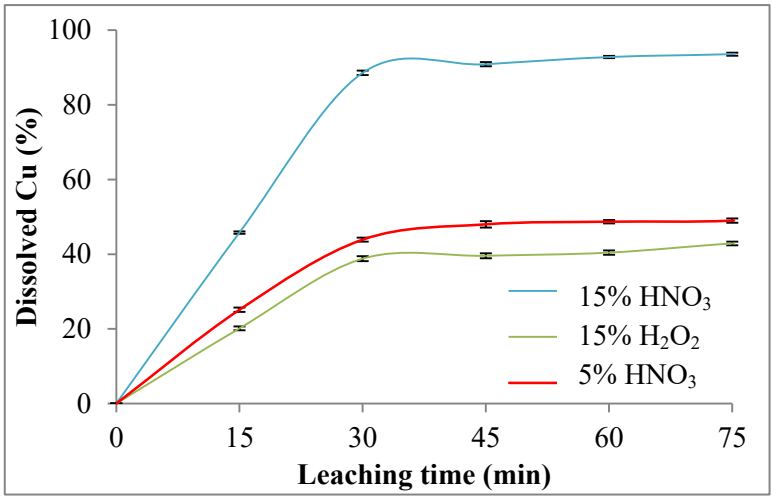

Figure 3.58- Leaching of Cu from WPCBs concentrate obtained by hammer milling and sieving under varying concentration of oxidant nitric acid and hydrogen peroxide [3M H_2SO_4, 140 ^oC, WPCBs size- 2.25 cm^2, pulp density 50 $g \cdot L^{-1}$]

3.5.2.1 Analysis of leached residue and samples used for leaching of copper

After, the leaching experiments the leached residue has been analyzed by using XRD technique. The **Figure 3.59** shows the XRD spectrum of DMA treated WPCBs, WPCBs obtained after hammer milling (enriched copper content) and respective residues after leaching. The XRD of DMA treated WPCBs showed the presence of major peaks of copper crystal (JCPDS File no. 04-0836). It may be deduced from the **Figure 3.59** that the intensity of the peaks is highest in case of DMA treated WPCBs compared to hammer milled WPCBs because of its higher copper content (~ 80% copper: please see **Section 3.3.3**). Further, it is also clear that after the leaching, the peak intensity decreases drastically showing that most of the copper has been leached out. Thus, the XRD results corroborate with the leaching study results. It is also notable that due to the presence of less fraction of glass fibre and other non-metallic compounds in DMA treated and hammer milled WPCBs, the noise in the XRD spectra near low 2-theta values is relatively less (**Figure 3.59**). Once the most of the copper is leached out, and a higher fraction of glass fibre and nonmetal are there, thus more noise in XRD spectra is seen near low 2-theta values due to the presence of amorphous phase(s).

The SEM-EDX analysis of the DMA treated WPCBs, hammer milled concentrate and residue obtained after leaching of DMA treated WPCBs has been carried out. Prior to the SEM analysis, DMA treated WPCBs have been crushed to fine size by using hammer mill. The **Figure 3.60** shows that most of the particles possess a flake and thin sheet-like morphology. Similar morphology has been registered by the copper particles after hammer milling as discussed in **Section 3.1.5.**

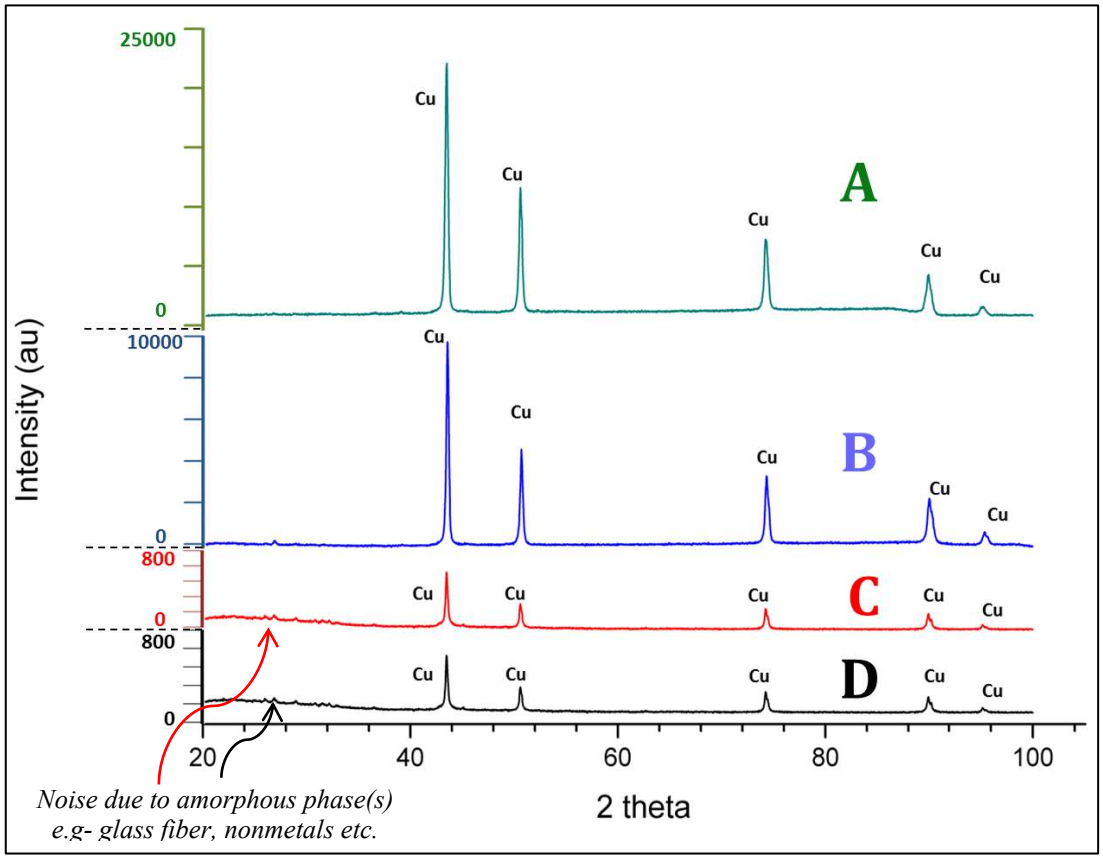

Figure 3.59- XRD analysis of (A) DMA treated WPCBs, (B) hammer milled WPCB's concentrate, (C) residues after leaching of DMA treated WPCBs, (D) Residues after leaching of Hammer mill treated WPCBs

EDS analysis of the selected area indicated the high fraction of copper (~70 wt%). These results are also in good agreement with the chemical analysis results of DMA treated WPCBs that showed the presence of ~80% copper (**Section 3.3.3**). The EDS analysis of a sample at different points showed that most of the particles are copper rich. Further, the elemental mapping of the selected area showed the presence of copper throughout all the particles (**Figure 3.61**). The SEM micrograph clearly indicated that copper particles are still having some adhered non-metallic fraction. These non-metallic fractions are easily distinguishable because of the charging effect experienced during

SEM (**Figure 3.60**). The described phenomena are more clearly visible in the SEM micrograph taken at higher magnifications (**Figure 3.62**).

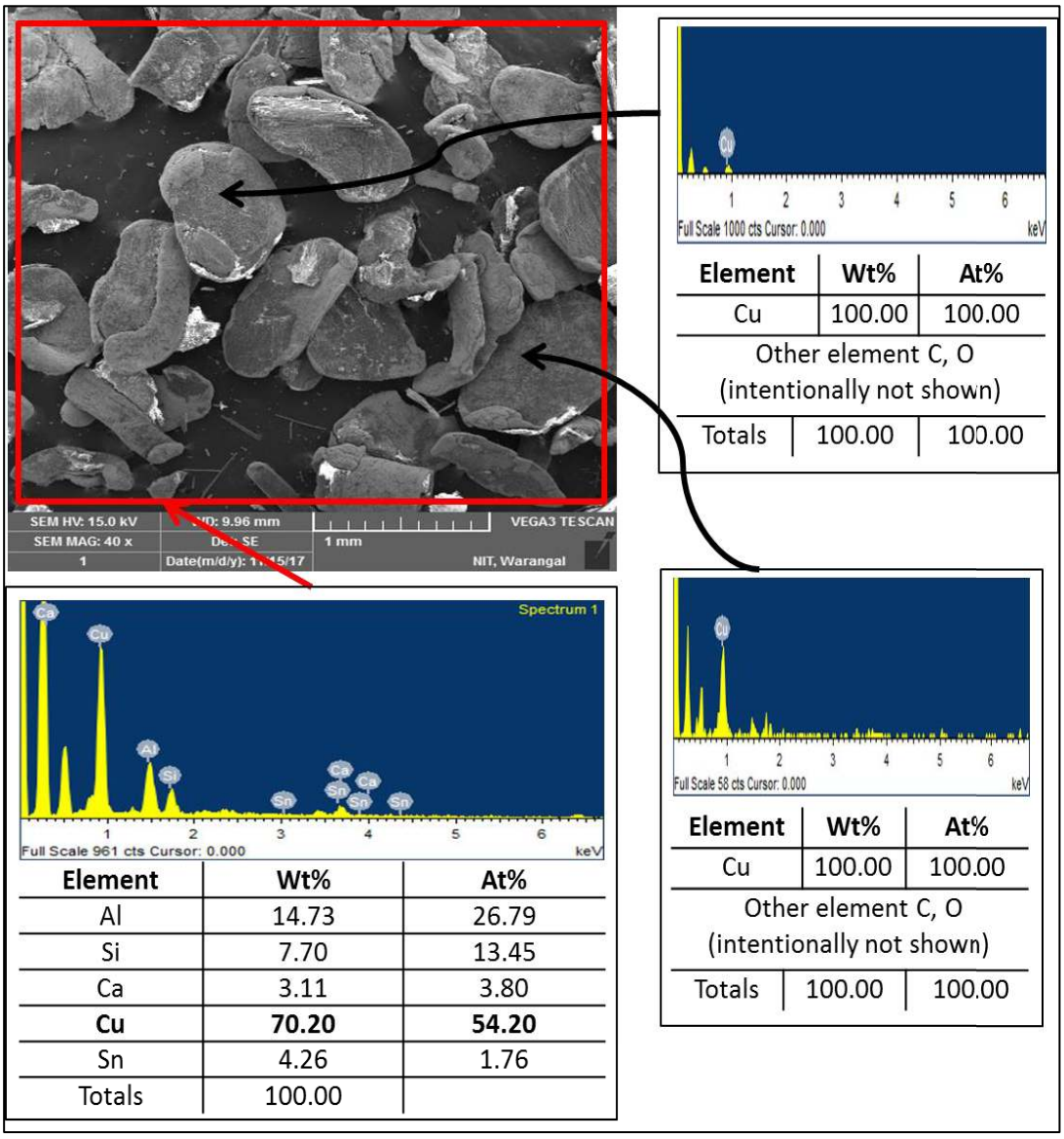

Element	Wt%	At%
Al	14.73	26.79
Si	7.70	13.45
Ca	3.11	3.80
Cu	**70.20**	**54.20**
Sn	4.26	1.76
Totals	100.00	

Element	Wt%	At%
Cu	100.00	100.00
Other element C, O (intentionally not shown)		
Totals	100.00	100.00

Element	Wt%	At%
Cu	100.00	100.00
Other element C, O (intentionally not shown)		
Totals	100.00	100.00

Figure 3.60- The SEM-EDS analysis of DMA treated WPCBs after crushing

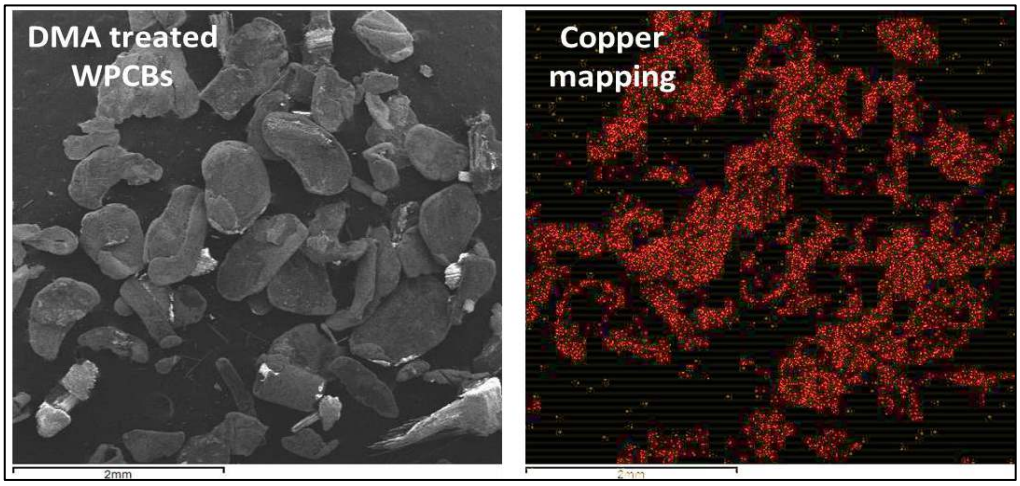

Figure 3.61- EDS mapping of copper on the selected area of SEM micrograph

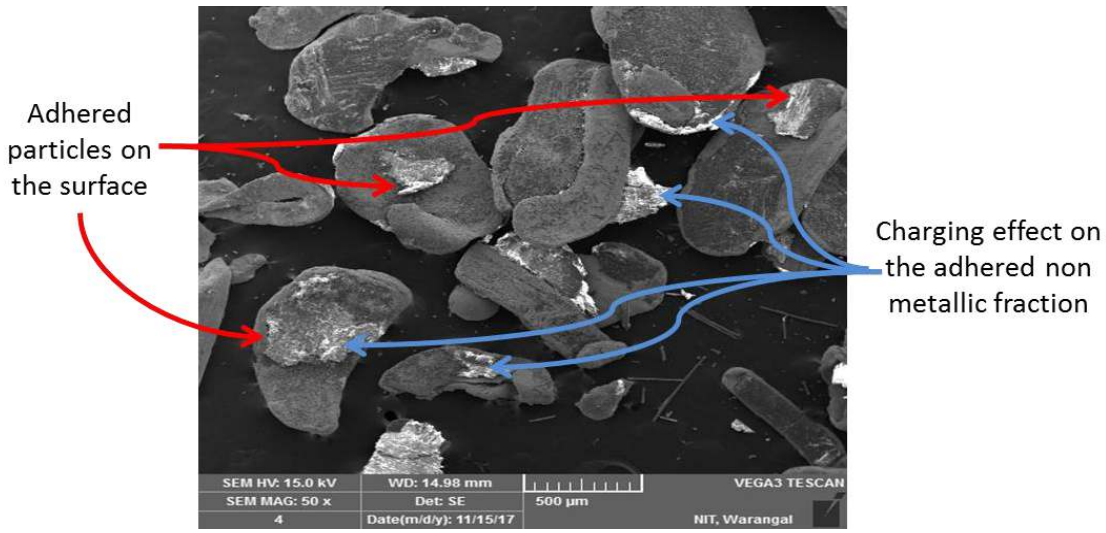

Figure 3.62- Adhered non-metallic particles on the surface of copper particles showing the charging effect

The SEM micrograph of the WPCB concentrate obtained by hammer mill showed particles of copper (**Figure 3.63-Point 3**) and unevenly distributed fibrous particles of different sizes (**Figure 3.63-Point 1,2**) throughout. The EDS analysis of the fibrous particle showed the presence of aluminium, calcium, silicon and oxygen which are the general constituents of glass fibre (**Figure 3.63-Point 1, 2**). It indicates that fibrous particles are mostly glass fibre and similar results had been observed during the

microscopic studies carried out in **Section 3.1.5.** The EDS analysis of the selected area showed the presence of ~35% copper particles along with aluminium, calcium, silicon and oxygen. This may be because the hammer milling and sieving enriched the copper content of WPCBs to 43 wt% copper (please see **Section 3.1**).

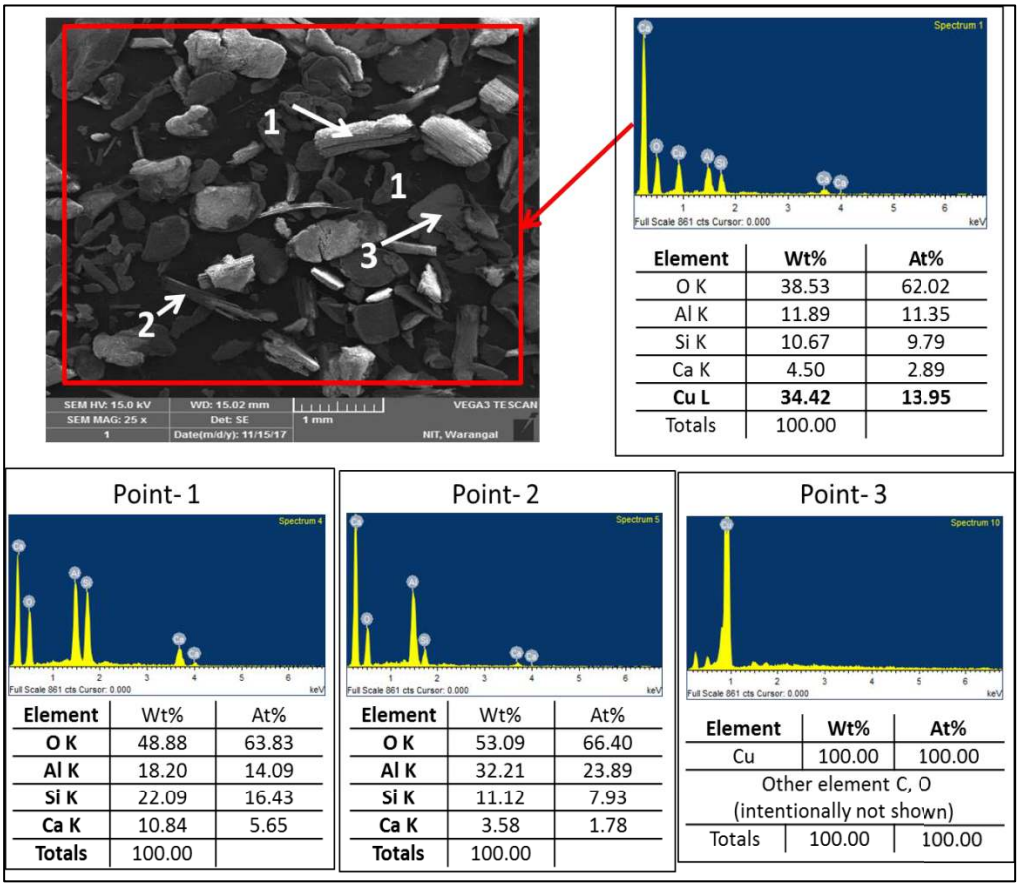

Figure 3.63- The SEM-EDS analysis of WPCB concentrate obtained after hammer milling and sieving

The SEM-EDS analysis of the residue generated after leaching of copper from DMA treated WPCBs showed the presence of glass fibre particles (**Figure 3.64**). A tiny needle and flake type particles have also been seen in the micrograph. These particles are the non-metallic fraction that was adhered to copper initially. Later, as the copper dissolved during the leaching these particles are liberated and thus formed tiny particles

of 10-30 µm. The EDS scan also showed negligible presence of copper in the residue and it confirms good leaching of copper.

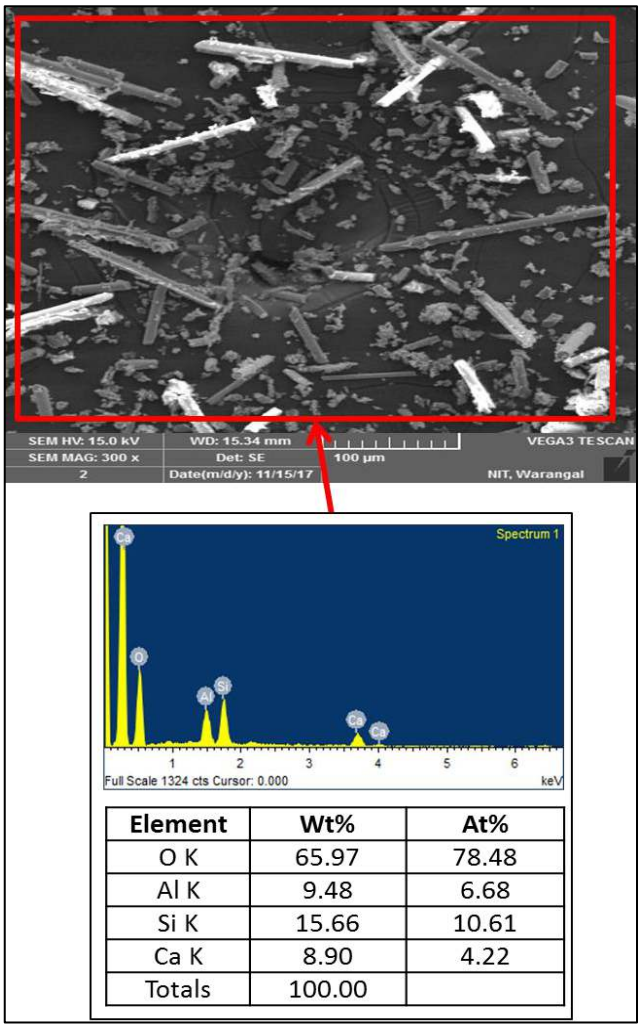

Element	Wt%	At%
O K	65.97	78.48
Al K	9.48	6.68
Si K	15.66	10.61
Ca K	8.90	4.22
Totals	100.00	

Figure 3.64- SEM-EDS analysis of residue after copper leaching from DMA treated WPCBs

The leachability test showed that pre-treatment by DMA liberates metal fraction more efficiently than the conventional hammer milling. Thus, it resulted in 95% copper recovery by using 5% of oxidant, while 94% copper recovery was seen from hammer mill treated WPCBs by using 15% oxidants.

Conclusions

The dissolution of HER from large size WPCBs showed that the time required for the successful delamination is considerably more. On the other hand, the copper leachability study on 'solvent treated WPCBs' showed improved leaching as compared to hammer milled WPCBs. The important results found from the present study are listed below-

- Investigation of delamination of large size WPCBs showed that more time is required for significant delamination.
- The study revealed that under condition *viz.,* WPCB:DMA- 3:10, 160 ^{o}C the WPCBs of 4 and 9 cm^2 could be delaminated within 3 and 5 h time, respectively.
- It is also found that WPCBs of larger size than 9 cm^2 (e.g., 16 cm^2) shows partial delamination after 7 h and a duration of 9 h is also not sufficient for complete delamination.
- This study confirms that for most efficient delamination and economical operation, relatively smaller size WPCBs (e.g.- 2.25 or 4 cm^2) are preferable as it results in complete delamination within a short duration.
- The leachability of copper from DMA treated and hammer milled treated WPCBs showed that DMA treated WPCBs are more suitable for copper recovery.
- The leaching studies by using oxidant hydrogen peroxide and nitric acid in presence of sulphuric acid showed that nitric acid is more suitable for copper leaching as it offers lower processing time and high recovery of copper.